REPORT DOCUMENTATION PAGE

AFRL-SR-AR-TR-06-0183

The public reporting burden for this collection of information is estimated to average 1 hour per response, including gathering and maintaining the data needed, and completing and reviewing the collection of information. Send comment information, including suggestions for reducing the burden, to Department of Defense, Washington Headquarters Serv 1215 Jefferson Davis Highway, Suite 1204, Arlington, VA 22202-4302. Respondents should be aware that notwith penalty for failing to comply with a collection of information if it does not display a currently valid OMB control number.
PLEASE DO NOT RETURN YOUR FORM TO THE ABOVE ADDRESS.

1. REPORT DATE *(DD-MM-YYYY)*	2. REPORT TYPE	3. DATES COVERED *(From - To)*
04/24/2006	Final	1 JAN 2003 - 31 DEC 2005

4. TITLE AND SUBTITLE

Advanced Techniques for MIMO Broadband Communications

5a. CONTRACT NUMBER

5b. GRANT NUMBER

F49620-03-1-0161

5c. PROGRAM ELEMENT NUMBER

6. AUTHOR(S)

Alex Haimovich

5d. PROJECT NUMBER

5e. TASK NUMBER

5f. WORK UNIT NUMBER

7. PERFORMING ORGANIZATION NAME(S) AND ADDRESS(ES)

New Jersey Institute of Technology
University Heights
Newark, NJ 07102-1982

8. PERFORMING ORGANIZATION REPORT NUMBER

9. SPONSORING/MONITORING AGENCY NAME(S) AND ADDRESS(ES)

Air Force Office of Scientific Research
4015 Wilson Blvd
Mail Room 713
Arlington, VA 22203

10. SPONSOR/MONITOR'S ACRONYM(S)

AFOSR

11. SPONSOR/MONITOR'S REPORT NUMBER(S)

12. DISTRIBUTION/AVAILABILITY STATEMENT

Distribution A; approved for public release; distribution unlimited

13. SUPPLEMENTARY NOTES

14. ABSTRACT

Multiple input multiple output (MIMO) systems can provide high diversity, high data rate or a mix of both, for wireless communications. This report combines both modes and suggests analyses and techniques that advance the state of the art of MIMO systems. Specifically, this report studies turbo space-time coding schemes for MIMO systems. Before the designs of turbo space-time codes are presented, a fundamental tool to analyze and design turbo coding schemes, the extrinsic information transfer (EXIT) chart method, is extended from the binary/nonbinary code case to coded modulation case. This extension prepares the convergence analysis for turbo space-time code. Turbo space-time codes with symbols pre-coded by randomly chosen unitary time variant linear transformations (TVLT) are investigated in this report. It is shown that turbo codes with TVLT achieve full diversity gain and good coding gain with high probability.

15. SUBJECT TERMS

16. SECURITY CLASSIFICATION OF:			17. LIMITATION OF ABSTRACT	18. NUMBER OF PAGES	19a. NAME OF RESPONSIBLE PERSON
a. REPORT	b. ABSTRACT	c. THIS PAGE	UU		
U	U	U			19b. TELEPHONE NUMBER *(Include area code)*

Standard Form 298 (Rev. 8/98)
Prescribed by ANSI Std. Z39.18

Advanced Techniques for MIMO Broadband Communications

US Dept. of Air Force F49620-03-1-0161

Final Report

1 Jan. 2003 – 31 Dec. 2005

submitted to Dr. Jon Sjogren

by

Alex Haimovich

NJIT

20060614025

Abstract

Multiple input multiple output (MIMO) systems can provide high diversity, high data rate or a mix of both, for wireless communications. This report combines both modes and suggests analyses and techniques that advance the state of the art of MIMO systems. Specifically, this report studies turbo space-time coding schemes for MIMO systems.

Before the designs of turbo space-time codes are presented, a fundamental tool to analyze and design turbo coding schemes, the extrinsic information transfer (EXIT) chart method, is extended from the binary/nonbinary code case to coded modulation case. This extension prepares the convergence analysis for turbo space-time code.

Turbo space-time codes with symbols precoded by randomly chosen unitary time variant linear transformations (TVLT) are investigated in this report. It is shown that turbo codes with TVLT achieve full diversity gain and good coding gain with high probability. The probability that these design goals are not met is shown to vanish exponentially with the Hamming distance between codewords (number of different columns). Hence, exhaustive tests of the rank and the determinant criterion are not required. As an additional benefit of the application of TVLT, with the removal of the constant modulation condition, it is proved that throughput rates achieved by these codes are significantly higher than the rates achievable by conventional space-time codes. Finally, an EXIT chart analysis for turbo space-time codes with TVLT is developed, with application to predicting frame error rate (FER) performance without running full simulation.

To increase the data rate of turbo-STC without exponentially increasing the decoding complexity, a multilevel turbo space-time coding scheme with TVLT is proposed. An iterative joint demapping and decoding receiver algorithm is also proposed.

For MIMO systems with a large number of transmit antennas, two types of layered turbo space-time (LTST) coding schemes are studied. For systems with low order modulation, a type of LTST with a vertical encoding structure and a low complexity parallel interference cancellation (PIC) receiver is shown to achieve close to capacity performance. For high order modulation, another type of LTST with a horizontal encoding structure, TVLT, and an ordered successive interference cancellation (OSIC) receiver is shown

to achieve better performance than conventional layered space-time coding schemes, where ordering is not available in the SIC detection.

Contents

List of Figures

3

Chapter 1

Introduction

Wireless communication has become pervasive in every day life, providing convenient ways to exchange information as well as supplying emergency help for its users through instant accessibility. Many applications such as cellular network, wireless LAN, digital video broadcasting, etc., have been evolving for years and new applications are still emerging. The constant demand for wireless communication is to make it faster, more reliable, and reaching farther.

One of the biggest obstacles for the development of wireless communication applications is the fading of the wireless channel. Fading is caused by the multipath of the transmitted signal arriving and adding either in phase or out of phase at the receiver, leading to random fluctuations in the amplitude and phase of the received signal.

To combat fading, multiple diversity technologies such as frequency diversity, temporal diversity, and spatial diversity, have been proposed. The core idea is to supply the receiver with multiple copies of the signal so that if one copy of the signal is deeply weakened by fading, the other copies may have a chance to be strong.

Among the diversity techniques, spatial diversity is the most preferable since it does not cause detection/decoding delay (as time diversity does) and does not cause bandwidth increase (as frequency diversity does). Spatial diversity is achieved by employing multiple antennas at either transmitter (transmit diversity) or at the receiver (receive diversity), or both. Wireless systems with multiple transmit/receive antennas are referred to as multiple input multiple output (MIMO) systems.

As studies advance, it is shown that MIMO systems are not just a tech-

nique to overcome the problems caused by fading. In fact, the studies in information theory [2], [3] show that MIMO systems can exploit the fading channels and achieve much higher capacity than which can be achieved on a nonfading, additive white Gaussian noise (AWGN) channel. Space-time coding (STC) [1] [4] [5], a joint design of coding, modulation, transmit and receive diversity, has been shown to be an efficient way to realize the big increase in the spectrum efficiency predicted by the information theory.

Turbo codes [6] are a class of codes that achieves near capacity performance. They have also been extended turbo space-time codes (turbo-STC) [7] [8] [9]. This report proposes and studies a new type of turbo-STC with the time varying linear transformation (TVLT) technique, which can be designed using a much simpler procedure, and achieves a higher data rate than existing turbo-STC.

In this chapter, the capacity of a MIMO channel is first presented, followed by the introduction of space-time coding and turbo coding. Finally, turbo space-time coding is introduced and the motivation for this report is presented.

1.1 MIMO Channel Capacity

Consider a MIMO system with n_T transmit and n_R receive antennas. The corresponding channel model is

$$\mathbf{r}(t) = \mathbf{H}\mathbf{x}(t) + \mathbf{n}(t), \tag{1.1}$$

where $\mathbf{r}(t)$ is the $n_R \times 1$ received signal vector at time interval t; $\mathbf{x}(t)$ is the $n_T \times 1$ vector of the transmitted signal; the energy of of each symbols in $\mathbf{x}(t)$ is E_s/n_T; $\mathbf{H} = \{h_{i,j}\}$ is the $n_R \times n_T$ channel gain matrix, whose elements $h_{i,j}, i = 1, ..., n_R, j = 1, ..., n_T$, are complex random variables due to fading; $\mathbf{n}(t)$ is zero-mean, additive white Gaussian noise (AWGN) with variance $N_0/2$ per dimension. The signal to noise ratio (SNR) is defined as E_s/N_0.

Consider a quasi static or block fading channel where the channel gain matrix $\mathbf{H}$ keeps constant within the transmission of a codeword (frame) but changes independently from one codeword to another codeword. The capacity of the MIMO channel (1.1) for a realization $\mathbf{H}$ is [2]

$$C\left(\mathbf{H}\right) = \log_2 \det \left(I + \frac{E_s}{n_T N_0} \mathbf{H}\mathbf{H}^\dagger \right)$$
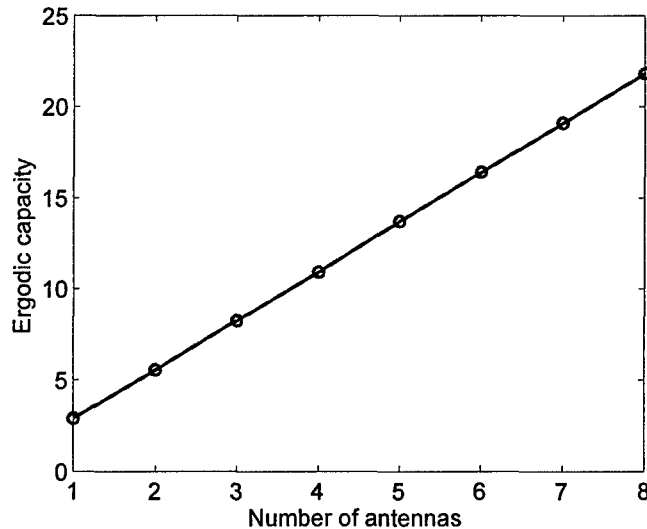
Figure 1.1: Example of linear increasing ergodic capacity with number of antennas.

where † denotes conjugate transpose. Since $\mathbf{H}$ is random, so does $C\left(\mathbf{H}\right)$. The capacity of the MIMO fading channel can be described as ergodic capacity

$$\overline{C} = \int \cdots \int C\left(\mathbf{H}\right) p\left(h_{1,1}, ..., h_{n_R, n_T}\right) dh_{1,1}...dv.$$

Consider a Rayleigh fading channel, where $\{h_{i,j}\}$ are zero mean complex Gaussian random variables with variance 1/2 per dimension. Also consider the cases where $n_T = n_R = n$. One example on the effect of the number of antennas on the ergodic channel capacity is shown in Figure 1.1 for SNR=10 dB. It is observed that the channel capacity increases linearly with the number of transmit and receive antennas. This figure demonstrates the advantage of using MIMO systems to increase the data rate.

The capacity of a MIMO fading channel can also be described by the outage probability, defined as the probability that the channel fails to support a required data rate C_0

$$P_o\left(C_0\right) \triangleq \Pr\left(C\left(\mathbf{H}\right) < C_0\right)$$

Outage probability is also the minimum frame error rate (FER) that can
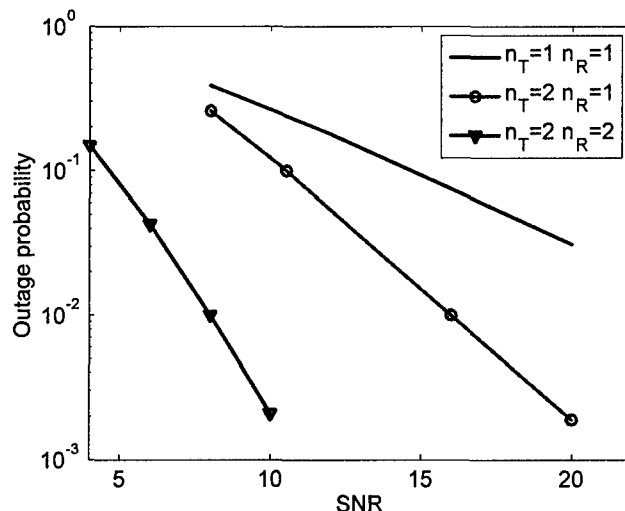
Figure 1.2: Outage probability comparison of channels with different number of transmit/receive antennas.

be achieved by any communication system over a certain fading channel. The outage probability versus SNR for $C_0 = 2$ b/s/Hz and for two MIMO channels with $n_T = 2$, $n_R = 1$, or 2×1, and $n_T = 2$, $n_R = 2$, or 2×2, are shown in Figure 1.2, with a comparison to the the outage probability of the 1×1 channel. It is observed that the slope of the outage probability curve of the 2×1 channel is twice as steep as that of the 1×1 channel, showing the effect of two order transmit diversity. The slope of the curve for the 2×2 channel is steeper than that of the 2×1 channel, showing the effect of additional receive diversity.

1.2 Space-time Codes

Encouraged by the studies in information theory, space-time coding [1] [4] [5] has been developed to realize the data rate and diversity improvement predicted by those studies. Space-time codes are multidimensional codes that generate multiple symbols at each time interval to be transmitted through multiple antennas. The design of space-time codes is guided by the rank criterion and the determinant criterion. Let $\mathbf{B}$ and $\mathbf{C}$ be an arbitrary pair of

9

$n_T \times L$ codeword matrices, where L is the length of the codeword. Further let $\mathbf{E} = \mathbf{B} - \mathbf{C}$ be the error matrix between $\mathbf{B}$ and $\mathbf{C}$. Then for the Rayleigh fading channel, the rank criterion says that the space-time code achieves r order transmit diversity, if and only if, for any pair of codewords $\mathbf{B}$ and $\mathbf{C}$, the rank of $\mathbf{E}$ is no less than r. The determinant criterion says that if r order transmit diversity is the design target, to achieve maximum coding gain, the minimum value of the product of the determinants of the all $r \times r$ principle cofactor of $\mathbf{E}\mathbf{E}^{\dagger}$ for all possible pair of codewords, should be maximized.

These two criteria reveal the fundamental conditions required for a code to achieve a desired order of diversity and coding gain. However, the two criteria are based on a pair of codewords. That is, every pair of codewords needs to be tested to find out whether the two criteria are satisfied. This leads to difficulty in the design of space-time codes and a computer search is usually needed [10].

The rate and diversity trade off is also studied in [1]. Let rn_R be the diversity advantage of the system. Assuming that the signal constellation Q has 2^b elements, the rate of transmission R satisfies

$$R \leq \frac{\log A_{bL}\left(n_T, r\right)}{L}$$

in bits per second per Hertz, where $A_{bL}\left(n_T, r\right)$ is the maximum size of a code length L and minimum Hamming distance r defined over an alphabet of size 2^{bL}. In a special case, if full diversity is the design target, then the maximum achievable rate is b b/s/Hz.

As an example, the FER performance of a 8 state space-time trellis code (STTC) [1] with 4-PSK modulation and rate 2 b/s/Hz is shown in Figure 1.3, with comparison to the outage probability. It is observed that both FER curves for 2×1 and 2×2 channels are parallel to those of the outage probability, demonstrating that full diversity is achieved by this STTC.

The decoding complexity for STC increases exponentially with the number of transmit antennas. When the number of transmit antenna is large (> 2), layered space-time codes (LSTC) [5] are usually used. In LSTC, the transmit antennas are divided into groups with smaller number (usually two) antennas. These groups are also referred to as layers. Independent STC are then applied in each layer. At the receiver, the signals from different layers are first separated by interference suppression techniques and then decoded.

10
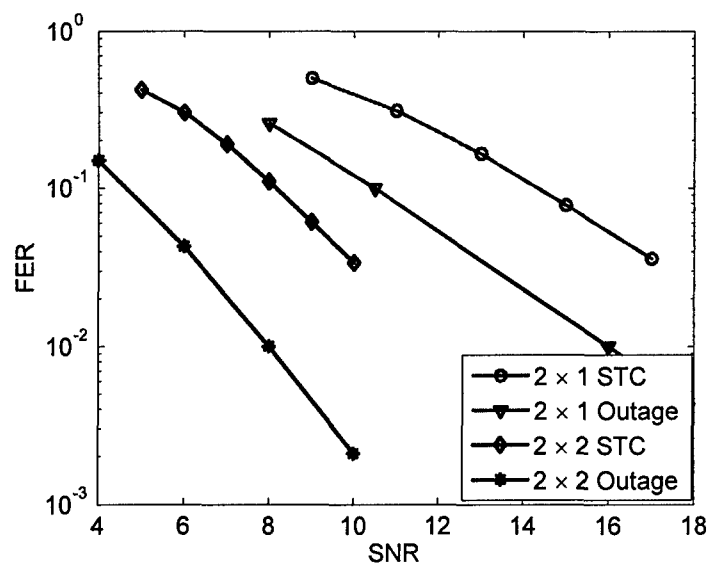
Figure 1.3: FER performance of a 8 state STTC [1] with comparison to the outage probability.

1.3 Turbo Codes

Turbo code [6] is a strong code that achieves near capacity performance. It is constructed by either parallel or serially concatenating two component convolutional/block codes. An example of a parallel concatenated turbo code is shown in Figure 1.4. In the encoder, the two component encoders are connected by a pseudo random interleaver which causes the generated codeword to be pseudo random also. This is the reason why turbo codes can achieve near capacity performance. Usually, the interleaver should be long enough for the turbo code to achieve the superior performance.

After being encoded by the two component encoders, the information bits and the parity bits may be mapped into nonbinary symbols. These types of schemes are referred to as turbo coded modulation [11] [12]. If the multiple symbols are generated after the mapping and transmitted through multiple antennas, the turbo code will be referred to as turbo space-time codes [7] [8] [9].

The decoder of the turbo code is also composed of two component soft input soft output (SISO) decoders, and works in an iterative fashion. During the iterations, the performance of the two component (SISO) decoders is enhanced by exchanging with each other the extrinsic information, or newly generated information, about the transmitted data. The convergence performance of the iterative decoder can be conveniently analyzed using the extrinsic information transfer chart (EXIT) [13] and other similar methods [14], [15].

1.4 Turbo Space-time Codes

Turbo space-time codes (turbo-STC) [7] [8] [9] are a special type of turbo codes that are applied to MIMO systems. As described in the last section, each pair of the codewords should be tested to see if the rank criteria and determinant criterion are satisfied. The test is, however, even more difficult to implement than the test for STTC. Since usually turbo space-time codes have a long interleaver (codeword), the number of codewords to test will be very, if not prohibitively, large. This is one of the problems to be dealt with in this report. A technique called time varying linear transformation (TVLT) will be applied to guarantee the full diversity of turbo-STC without testing each pair of the codewords.

12
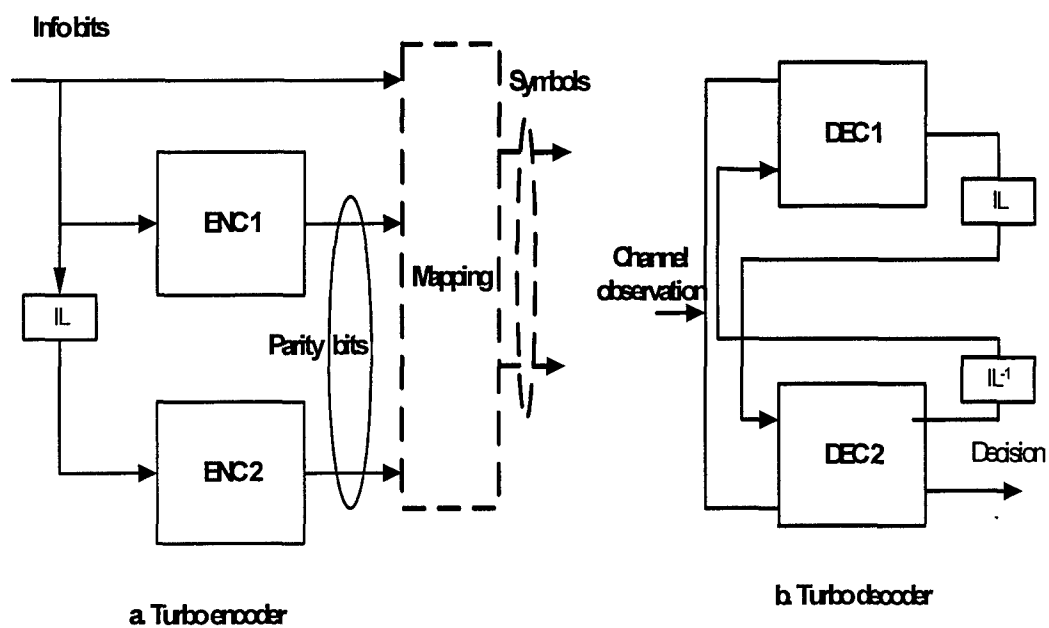
Figure 1.4: Structure of the encoder and decoder of a parallel concatenated turbo code.

13

The EXIT chart method is an accurate and low complexity method used to predict the performance of turbo codes. But it is not useful for conventional turbo-STC for the reasons that will be explained later in section 3.3.4 of this report. With TVLT, this method can be again applied. Generating EXIT charts for turbo space-time codes with TVLT is another problem to be investigated in this report.

1.5 Outline of the report

This report is organized as follows. First the EXIT chart is extended from binary turbo codes to turbo coded modulation in Chapter 2, which prepares the tool for analyzing the convergence of turbo space-time codes. In Chapter 3, the technique of TVLT is applied to turbo-STC. It will be shown that TVLT guarantees full diversity, and the large minimum Hamming distance of turbo space-time codes will guarantee good coding gain. The convergence analysis of turbo-STC is also presented in Chapter 3. Multilevel turbo-STC and layered turbo-STC will be presented in Chapters 4 and 5, respectively. The summary and anticipated future work are presented in Chapter 6.

Chapter 2

Convergence Analysis of Turbo Trellis Coded Modulation

Convergence analysis of iterative decoding algorithms for turbo codes has received much attention recently due to its useful application in predicting code performance, its ability to provide insights into the encoder structure, and its usefulness in helping with the code design. Several methods have been proposed to analyze the convergence of the iterative decoders for binary turbo codes [13–15]. In particular, the extrinsic information transfer (EXIT) method [13] has created a lot of interest. The EXIT method has been extended to the analysis of nonbinary turbo codes in [16].

Turbo trellis coded modulation (TTCM) [11, 12], conjoins signal mapping techniques, such as Ungerboeck's signal space partition [17], with turbo coding, to achieve significant coding gains without increasing bandwidth. However the need for signal mapping makes the encoder structure more complex to design and analyze than binary turbo codes. Hence the convergence analysis is a very important tool for the design and comparison of TTCM schemes.

In TTCM, systematic bits and parity bits are usually mapped to and transmitted as a single symbol. At the receiver, a symbol decoder is used instead of a binary decoder [11,12]. Consequently, the systematic information and extrinsic information are not naturally separated as in binary turbo codes. The separation is not necessary for carrying out the decoding. It is, however, needed for generating the EXIT chart. Due to mixing of the systematic and extrinsic information, the approach for generating the EXIT chart for binary decoders, or even for nonbinary decoders [16], can not be

directly applied to TTCM.

In this chapter, the EXIT chart for TTCM is developed by showing a way to explicitly separate the systematic information from the extrinsic information. To be specific, the analysis based on the TTCM codes introduced in [11] is developed. The application of the proposed method to other structures is fairly straightforward. Furthermore, the EXIT chart method presented in this chapter will be used to analyze the convergence performance of the turbo space-time codes.

The rest of the chapter is organized as follows. In section 2.1 the structure of TTCM is briefly introduced and the EXIT chart for TTCM is developed in section 2.2. Several examples are used to illustrate and demonstrate the proposed method in section 2.3. Conclusions are drawn in section 2.4.

2.1 TTCM Structure

2.1.1 Encoder Structure

The structure of the TTCM encoder [11] is presented in Figure 2.1. Assuming a 2^{m+1} constellation, at each time interval k, a symbol is transmitted representing m information bits $\mathbf{b}[k] = \{b[k,i]\}_{i=0}^{m-1}$. Of the m bits, possibly only $\widetilde{m}$ bits $\{b[k,i]\}_{i=0}^{\widetilde{m}-1}$, are encoded, whereas the other $(m - \widetilde{m})$ uncoded bits are input directly to the symbol mapper. The turbo encoder consists of two rate $\widetilde{m}/(\widetilde{m}+1)$ component recursive systematic convolutional (RSC) encoders, which are connected by a symbol ($\widetilde{m}$ bits) interleaver. These $\widetilde{m}$ encoded bits, are labeled for later use as the $2^{\widetilde{m}}$-ary level symbol $d[k] \triangleq \sum_{i=1}^{\widetilde{m}} b[k,i]2^{i-1}$.

The parity bits $c_1[k]$ and $c_2[k]$ from the two component encoders (the parity bits from the encoder with interleaved input are deinterleaved to their original order) are alternatively punctured, and the surviving parity bit $c[k]$ is mapped together with the m data bits to M-QAM or MPSK symbols $s[k]$, and transmitted.

b[k, m−1]

b[k, m̃]   uncoded bits

b[k, m̃−1]

b[k, 0]

ENC1 $c_1[k]$

IL

ENC2 $c_2[k]$ Punc-turing $c[k] =$ $c_1[k]$ or $c_2[k]$

Mapp-ing $s[k]$
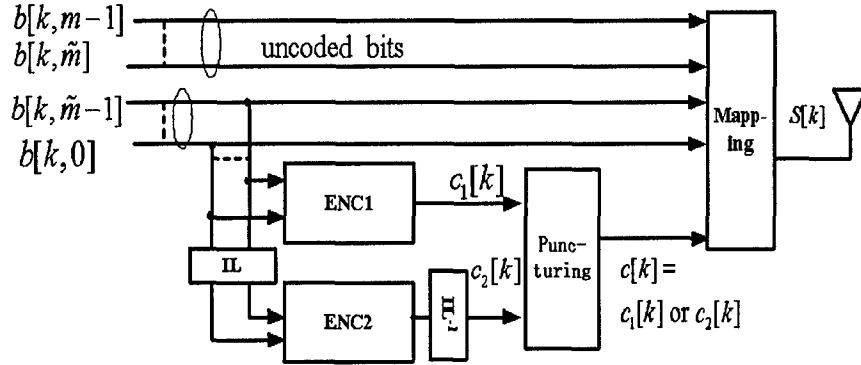
Figure 2.1: Structure of TTCM encoder with $\tilde{m}$ coded bits and $m - \tilde{m}$ uncoded bits.

2.1.2 Decoder Structure

The structure of the TTCM decoder is depicted in Figure 2.2. The decoder consists of two symbol maximum *a posteriori* (MAP) decoders, which exchange information about the symbols $\{d[k]\}$ formed by the *encoded* data bits. Of course, no information on uncoded bits is exchanged. Hence in TTCM, the systematic information represents the $\tilde{m}$ coded bits $\{b[k, i]\}_{i=0}^{\tilde{m}-1}$. Let the TTCM codeword consist of N symbols $(s[1], s[2], \dots, s[N])$. The channel observation is given by

$$y[k] = s[k] + n[k], \tag{2.1}$$

where $n[k]$ is zero mean white Gaussian noise with variance σ^2. The signal to noise ratio (SNR) is then defined as $E[\|s[k]\|^2]/\sigma^2$.

Due to fact that the symbol $s[k]$ embodies both the systematic and parity bits, and consequent to the alternative puncturing of the parity bits, it is shown in [11] that half of the information exchanged between component decoders contains systematic information and half does not. Unlike the binary turbo code case, the *a posteriori* probabilities (APP) $\mathbf{L}_p[k] \triangleq \{\log P(d[k] = u|\mathbf{y})\}_{u=0}^{2^{\tilde{m}}-1}$ computed by either component decoder can be decomposed into only two parts. The first part is the *a priori* input $\mathbf{L}_a[k] \triangleq \{\log P(d[k] = u)\}_{u=0}^{2^{\tilde{m}}-1}$, passed from the other decoder. The second part is different for two

cases: (i) at time interval k, $s[k]$ contains the parity bit from the *corresponding* component encoder; (ii) at time interval k, $s[k]$ contains parity bit from the *other* component encoder. For case (ii), the second part only contains the newly generated extrinsic information output, denoted as $\mathbf{L}_e^{out}[k]$. For case (i) however, the second part is a mixture of the extrinsic information and systematic information, denoted as $\mathbf{L}_{es}^{out}[k]$. That is,

$$\mathbf{L}_p[k] = \begin{cases} \mathbf{L}_a[k] + \mathbf{L}_{es}^{out}[k], & k \in \text{case (i)} \\ \mathbf{L}_a[k] + \mathbf{L}_e^{out}[k], & k \in \text{case (ii)} \end{cases}, \tag{2.2}$$

Accordingly, the *a priori* input to each component decoder $\mathbf{L}_a[k]$ is, for case (i), only extrinsic information, denoted as $\mathbf{L}_e^{in}[k]$; and is, for case (ii), the mixture of both extrinsic information and systematic information, denoted as $\mathbf{L}_{es}^{in}[k]$. That is

$$\mathbf{L}_a[k] = \begin{cases} \mathbf{L}_e^{in}[k], & k \in \text{case (i)} \\ \mathbf{L}_{es}^{in}[k], & k \in \text{case (ii)} \end{cases}. \tag{2.3}$$
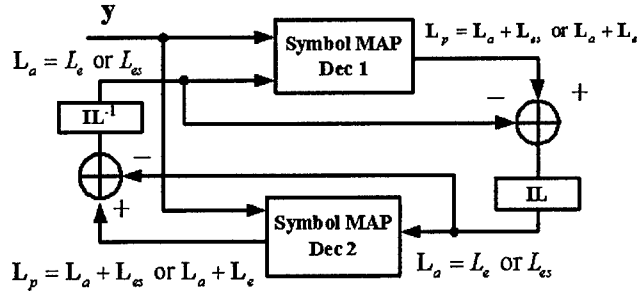
Figure 2.2: The structure of a TTCM decoder with two component MAP decoders.

2.2 EXIT Charts for TTCM

The EXIT chart is a tool for studying the convergence of turbo decoders without simulating the whole decoding process. The chart is generated by a single component decoder by mimicing the *a priori* input (as if it is generated

18

by the other decoder) and measuring the output. It is found in [13–15] that for binary MAP decoders, when the random interleaving sufficiently deep, the *a priori* inputs (the extrinsic information passed from the other component decoder), $\lambda = \log \frac{P(b=1)}{P(b=0)}$, for each data bit b, are mutually independent and can be closely modeled as independent, identically distributed (i.i.d.) random variables that follow the same Gaussian distribution $p(\lambda|b)$. In addition, the mean value μ and variance σ^2 of $p(\lambda|b)$ satisfy the consistency condition $\mu = \frac{1}{2}\sigma^2$. Then $p(\lambda|b)$ is determined by only one parameter, either μ or σ^2. So to generate λ with a given mutual information content $A = I(\lambda; b)$, the parameter of $p(\lambda|b)$, μ (or σ^2) can be found by

$$
\begin{aligned}
A &= I(\lambda; b) \\
&= \frac{1}{2} \sum_{x=0,1} \int_{-\infty}^{+\infty} p(\lambda|b = x) \\
&\qquad \cdot \log \frac{2 \cdot p(\lambda|b = x)}{p(\lambda|b = 0) + p(\lambda|b = 1)} d\lambda \\
&\triangleq J(\mu)
\end{aligned}
\tag{2.4}
$$

and

$$
\mu = J^{-1}(A). \tag{2.5}
$$

The above procedure is used to generate the *a priori* input to a binary MAP decoder. For TTCM, the component decoder is a nonbinary symbol decoder, and the *a priori* has different contents in actual operation for the two different cases shown in (2.3). To mimic the *a priori* input $\mathbf{L}_e^{in}[k]$ for $k \in$ case (i), which contains only the extrinsic information generated by the other decoder, the assumption proposed in [16] that the log-likelihood ratios $\{\lambda[k, i] = \log \frac{P(b[k,i]=1)}{P(b[k,i]=0)}\}_{i=0}^{\widetilde{m}-1}$ for the bits $\{b[k, i]\}_{i=0}^{\widetilde{m}-1}$ composing the nonbinary symbol $d[k]$ are i.i.d. Gaussian random variables, is adopted. Thus $\{\lambda[k, i]\}_{i=0}^{\widetilde{m}-1}$ can be generated as in the binary turbo code case, with the value A in (2.5) set to $A = I_e^{in}/\widetilde{m}$, where I_e^{in} is the desired mutual information between $\mathbf{L}_e^{in}[k]$ and $d[k]$, i.e., $I_e^{in} = I(\mathbf{L}_e^{in}[k]; d[k])$. The term $\mathbf{L}_e^{in}[k] = \{\log P(d[k] = u)\}_{u=0}^{2^{\widetilde{m}}-1}$ can be calculated using $\{\lambda[k, i]\}_{i=0}^{\widetilde{m}-1}$.

For $k \in$ case (ii), the *a priori* is a mixture of both extrinsic and systematic information $\mathbf{L}_{es}^{in}[k]$ as shown in (2.3). Before generating the mixture, it is needed to find out what the systematic information will be, even if does not appear explicitly during the decoding process in TTCM. In binary turbo

19

coding, the systematic information is the information associated with the channel observation of the systematic bit. This should also be the case in TTCM, although each sample of the channel observation contains both systematic bits (symbol), uncoded bits and parity bits. That is, the systematic information about symbol $d[k]$ should be computed as

$$P(d[k] = u|y[k]) = \sum_{b[k,\tilde{m}+1]=\{0,1\}} \cdots \sum_{b_{k,m}=\{0,1\}} \sum_{c_k=\{0,1\}} P(y[k]|s[k] =$$

$$\text{mapping}(d[k] = u, b[k, \tilde{m}+1], ..., b[k,m], c[k])), \quad u = 0, ..., 2^{\tilde{m}} - 1. \quad (2.6)$$

Equation (2.6) can also be rewritten in the form of a vector of log-likelihood values as

$$\mathbf{L}_s[k] = \{\log P(d[k] = u|y[k]), u = 0, ..., 2^{\tilde{m}} - 1\}. \quad (2.7)$$

Now the systematic information $\mathbf{L}_s[k]$, for $k \in$ case (ii), has been explicitly formed. To generate the mixture, it is also necessary to generate for each $k \in$ case (ii) a vector extrinsic part $\mathbf{L}_e^{in}[k]$ with $I(\mathbf{L}_e^{in}[k]; d[k]) = I_e^{in}$, in the same way as for case (i). Thus, the mixture $\mathbf{L}_a[k] = \mathbf{L}_{es}^{in}[k]$ is generated as the combination of extrinsic information and systematic information, i.e., $\mathbf{L}_a[k] = \mathbf{L}_e^{in}[k] + \mathbf{L}_s[k]$. To conclude, the *a priori* input to the TTCM component decoder is generated as

$$\mathbf{L}_a[k] = \begin{cases} \mathbf{L}_e^{in}[k], & k \in \text{ case (i)} \\ \mathbf{L}_e^{in}[k] + \mathbf{L}_s[k], & k \in \text{ case (ii)}. \end{cases} \quad (2.8)$$

Next the measurement of the extrinsic information at the output of the TTCM component decoder is discussed. According to (2.2), for $k \in$ case (i) the extrinsic information is mixed with systematic information. However, the systematic information can be formed using (2.6) and (2.7) and then subtracted. That is, the extrinsic information $\mathbf{L}_e^{out}[k]$ for data symbol $d[k]$ is obtained as:

$$\mathbf{L}_e^{out}[k] = \begin{cases} \mathbf{L}_p[k] - \mathbf{L}_a[k] - \mathbf{L}_s[k], & k \in \text{case(i)} \\ \mathbf{L}_p[k] - \mathbf{L}_a[k], & k \in \text{ case (ii)}. \end{cases} \quad (2.9)$$

Due to the independence assumption, $\{\mathbf{L}_e^{out}[k]\}_{k=0}^{N-1}$ are mutually independent and follow the same distribution $p_e(\mathbf{L}_e^{out}|d)$. The multi-dimensional joint distribution $p_e(\mathbf{L}_e^{out}|d)$ is obtained by measuring the histogram of $\mathbf{L}_e^{out}$

20

using its samples $\{\mathbf{L}_e^{out}[k]\}_{k=0}^{N-1}$. Then the mutual information between the extrinsic output and the transmitted symbol d is computed as

$$
\begin{aligned}
I_e^{out} &= I(\mathbf{L}_e^{out}; d) \tag{2.10} \\
&= \frac{1}{2^{\tilde{m}} - 1} \sum_{u=0}^{2^{\tilde{m}}-1} \int p_e^{out}(\xi | d = u) \cdot \\
&\quad \log \frac{(2^{\tilde{m}} - 1) \cdot p_e^{out}(\xi | d = u)}{\sum_{u=0}^{2^{\tilde{m}}-1} p_e^{out}(\xi | d = u)} d\xi.
\end{aligned}
$$

The EXIT chart for TTCM is then generated by measuring the output mutual information I_e^{out} as a function of a family of inputs with specified mutual information I_e^{in} and channel observation of specified SNR, $I_e^{out} = f(I_e^{in}, \text{SNR})$.

The overall block diagram for generating EXIT charts for TTCM schemes is illustrated in Figure 2.3.
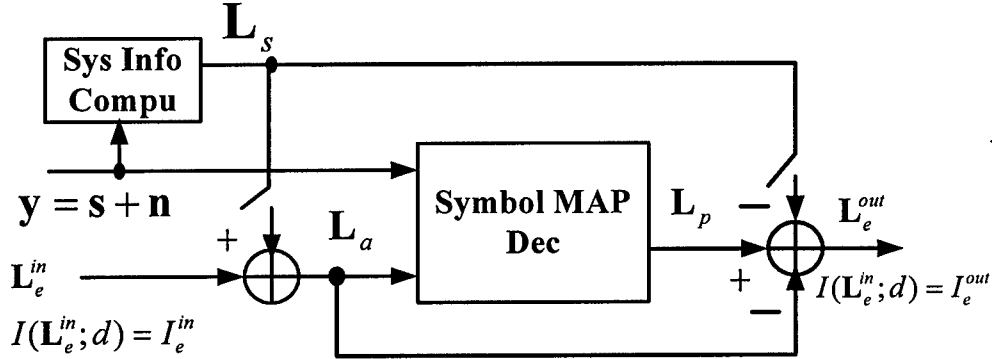
Figure 2.3: The block diagram to generate EXIT charts for a TTCM MAP decoder.

2.3 Applications

In this section, a few examples are presented to illustrate the applications of the proposed EXIT chart method for TTCM.

21

2.3.1 Role of Primitive Feedback Polynomials

The proposed EXIT chart method is applied to analyze and compare two TTCM schemes. The first code is from [11], Table I, first row. This is an 8-state code with 8-PSK modulation, and $m = \widetilde{m} = 2$. The second code has the same structure but the parameter $H^0(D)$ in the first row of table I [11] is changed from $(11)_8$ to $(13)_8$. This changes the feedback polynomial of the component encoder from nonprimitive to primitive. Hence, a primitive code and a nonprimitive code are compared. The data rates of both codes are 2 b/s/Hz.

The EXIT charts for these two codes are presented in Figure 2.4, for channel SNR 5.8 dB, 6.2 dB and 7.0 dB, respectively. For schemes with symmetric structure (identical component encoders/decoders), only the EXIT chart for one of the decoders needs to be plotted. In the figure, the abscissa is $I_e^{in} = I(\mathbf{L}_e^{in}; d)$ in bits, and the ordinate is $I_e^{out} = I(\mathbf{L}_e^{out}; d)$ also in bits.

It is observed from the figure that for both codes, the curves of SNR=5.8 dB intersect with the y = x line, which means that at some point during the iteration the decoder can no longer increase the extrinsic information compared to the input. In this case the decoding will fail no matter how many iterations are run. Both curves for SNR = 6.2 dB are just a little above the y = x line, which means for that any SNR $\geqslant$ 6.2 dB, the extrinsic information output at the component decoder will always be better than the input, and the decoder will converge to the correct codeword with high probability. That is, the convergence threshold of these two codes is about 6.2 dB. The simulated bit error rate (BER) performance curve is shown in Figure 2.5 after 8 iterations. The length of the interleaver is 1024. It is observed that the BER curve actually turns down sharply at about 6.2 dB, which verifies the convergence threshold predicted by the EXIT chart.

In Figure 2.4, it is also observed that the curves of the primitive code are always higher than the nonprimitive code, especially at higher values of input mutual information. This implies a faster convergence speed, which agrees with the observation in binary turbo codes that codes with primitive feedback polynomial have faster convergence speed than the nonprimitive ones [15]. This observation is also verified by the BER curves in Figure 2.5, where with the same number of iterations, the performance of the primitive code is always better than that of the nonprimitive code. So this example suggests that in TTCM, primitive codes should be favored over nonprimitive codes.

Figure 2.4: EXIT charts comparison of two codes with primitive and non-primitive feedback polynomials.
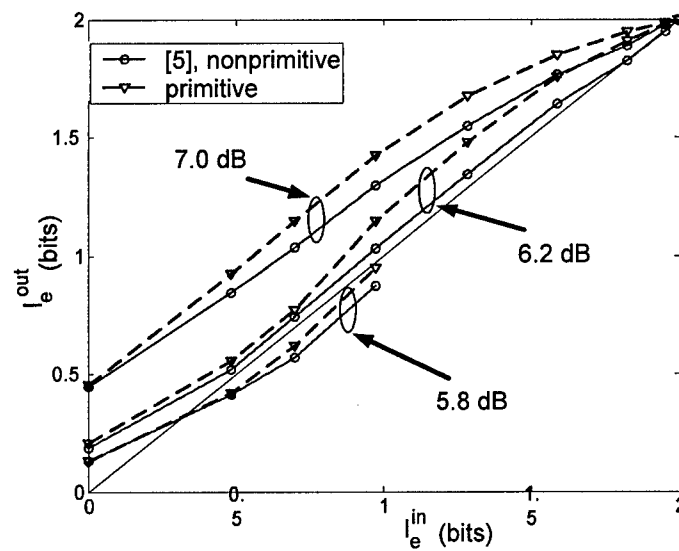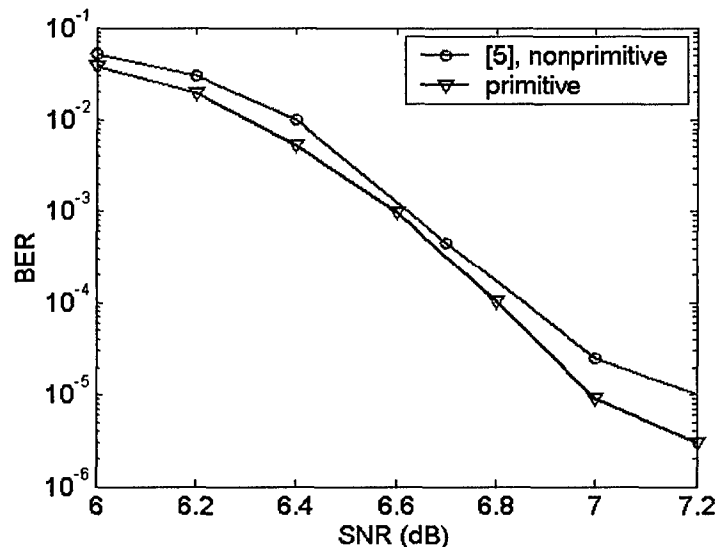
Figure 2.5: BER comparison of two codes with primitive and nonprimitive feedback polynomials.

2.3.2 Analysis and design of TTCM schemes with uncoded bits

In this subsection, the method to use the proposed EXIT scheme to predict the performance of TTCM schemes with uncoded bits is shown. It is also shown how the system design can be improved by examining the EXIT chart.

First the 3 b/s/Hz, 16 QAM scheme in [11], with 8-state component codes is studied. In this scheme three bits are transmitted at each time interval but only two are coded. Consequently, there are two parallel branches for each transition in the trellis. The goal of the analysis is to find at what SNR the system can achieve a given bit error rate (BER), e.g., BER=10^{-5}. First according to the set partition diagram, [17] Figure 5, the distance between the parallel transitions is found to be $d_p = \sqrt{8} \cdot \Delta_0$, where Δ_0 is the minimum

distance between the points of 16 QAM and $\Delta_0 = 2/\sqrt{10} \cdot E_s$. Since

$$BER = Q\left(\sqrt{\frac{d_p^2}{N_0}}\right) = Q\left(\sqrt{\frac{8\Delta_0^2}{N_0}}\right) \qquad (2.11)$$

$$= Q\left(\sqrt{\frac{16E_s}{10N_0}}\right)$$

the required SNR is

$$\frac{E_s}{N_0} = \frac{10}{16}\left(Q^{-1}\left(BER\right)\right)^2 \qquad (2.12)$$

For BER=10^{-5}, the required channel SNR is about 10.5 dB. Next, the EXIT chart for the underlying turbo code at this SNR is generated and shown in Figure 2.7. From the figure it is observed that EXIT curve is far above the y=x line and the opening between the EXIT curve and the y=x line is very large, which means the decoder has converged at SNR=10.5 dB and the convergence speed is fast. The convergence threshold for this code is found as 9.6 dB, as also shown in Figure 2.7. Obviously, the BER performance of the whole system is dominated by the BER of the uncoded bit and the performance of BER=10^{-5} will be achieved at about 10.6 dB. This can be verified by checking the BER performance curve in [11].

The analysis also suggests the turbo code used is too strong, and a code with lower state complexity may be used. In Figure 2.6 A 4-state component code is proposed as an alternative. The EXIT chart for this code is also shown in Figure 2.7, for SNR=10.5 dB. It is observed that although the curve for the 4-state code is lower than the 8-state code, the opening is still very wide and suggests a good convergence speed. Hence, the complexity of the decoder can be lowered with little performance loss.

2.3.3 Performance Analysis of TTCM over Fading Channel

The convergence analysis of the TTCM schemes over AWGN channel also leads to convenient, accurate prediction of the performance of the TTCM schemes over block fading channels. The frame error rate (FER) performance is just the probability that the channel gain falls below the convergence threshold of the TTCM code. For the block Rayleigh fading channel,
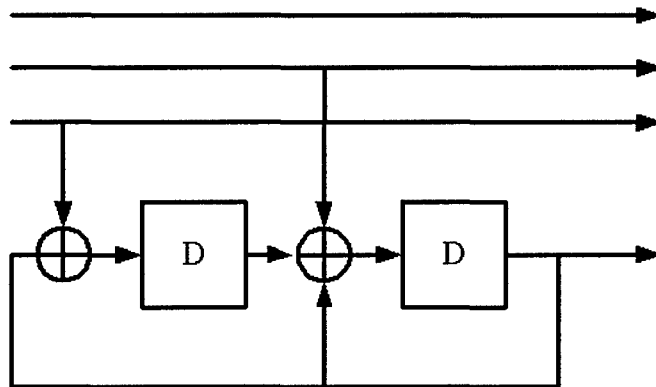
Figure 2.6: An alternative 4-state component encoder for the 3 b/s/Hz, 16QAM scheme.
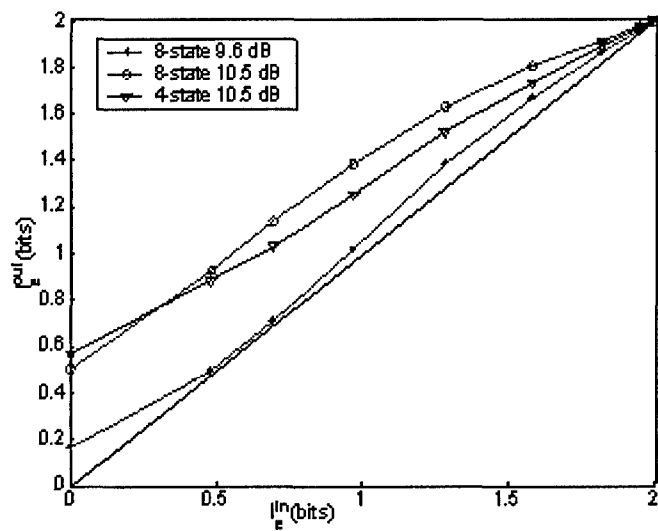
Figure 2.7: EXIT charts for two 16 QAM, 3 b/s/Hz TTCM schemes with 8-state and 4-state component encoder, respectively.

the channel model is

$$y[k] = h \cdot s[k] + n[k], \tag{2.13}$$

where h is the complex channel gain modelled as a zero mean, unit variance Gaussian random variable. The definition of other variables are the same as in (2.1). Denote the channel SNR $\gamma = \frac{E_s}{N_0}$. The effective channel SNR under channel gain h is $\xi = \gamma \cdot |h|^2$. It is obvious ξ follows an exponential distribution. The probability density function of γ is

$$p(\xi) = \frac{1}{\gamma} \exp(-\xi/\gamma) \tag{2.14}$$

Denote the SNR required by the TTCM code to converge γ_{th}. Then the FER is

$$\begin{aligned} P_e &= P(\gamma < \gamma_{th}) \\ &= \int_0^{\gamma_{th}} \frac{1}{\gamma} \exp(-\xi/\gamma) d\xi \\ &= 1 - \exp(-\gamma_{th}/\gamma) \end{aligned} \tag{2.15}$$

The convergence threshold for the primitive 2 b/s/Hz TCM code discussed in subsection 2.3.1 is $\gamma_{th} = 6.2$ dB. The predicted FER performance versus SNR is plotted in Figure 2.8. The FER performance obtained by full simulation is also shown in the figure for comparison. It is observed that the two curves almost overlap each other, indicating an accurate match.

2.4 Chapter Summary

The method to generate the EXIT chart for TTCM decoders is proposed. The accuracy and usefulness of this method has been verified through examples. Since the complexity of generating EXIT charts is significantly lower than a full simulation, the proposed method supplies a convenient way to compare various TTCM schemes as well as to verify and compare new designs.
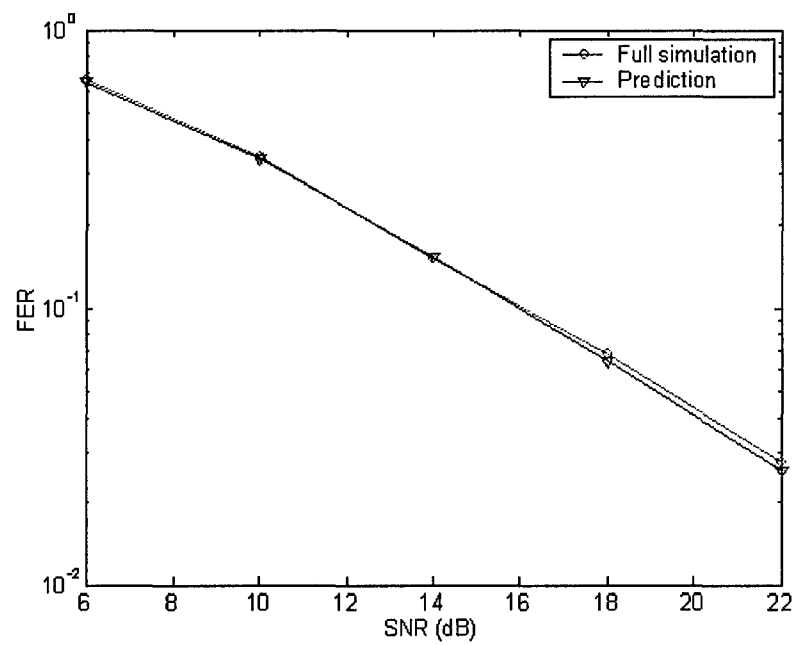
Figure 2.8: Comparison of the simulated and predicted FER performance for a 2 b/s/Hz TCM code.

Chapter 3

Turbo Space-time Coding with Time Varying Linear Transformations

The invention of space-time codes [1] has been seminal in the advance of multiple input multiple output (MIMO) techniques. Space-time codes apply to multiple transmit antennas to achieve both diversity and coding gains over fading channels. However, the design of full diversity codes with good coding gain has been challenging. One of the difficulties has been the lack of effective design tools to meet specified diversity and coding gains criteria. In most cases, to ensure meeting diversity and gain specifications [1], exhaustive checks are required of all pairs of codewords, and numerical simulations are needed to evaluate overall performance.

Turbo space-time codes (STC) are specially designed turbo codes for MIMO channels that can achieve much higher coding gains than conventional space-time trellis codes. Existing schemes such as [7], [8], and [9], etc., display similar performance but have distinct encoder/decoder structures. For all turbo-STC, exhaustive tests are required to ensure full diversity. If the test fails, the codes have to be adjusted, and the testing procedure is restarted.

The main goal in this chapter is to simplify the design of full diversity turbo space-time codes. Phase sweeping [18–20], a precursor to space-time codes, guarantees full diversity, but no coding gain. It still attracts attention both in academia and industry [21,22]. The approach taken in this report is a technique related to phase sweeping and is referred to as *time varying linear transformation* (TVLT) [23]. TVLT offers more flexibility for integration in

29

space-time codes than phase sweeping. With TVLT, transmitted symbols are modified by a unitary transformation represented by a unitary matrix. The elements of the matrix are in part selected at random and in part designed to meet the unitary conditions. The transformation changes at each time interval, but the sequence of transformations is known to both the transmitter and the receiver. A previous attempt of applying TVLT to turbo space-time codes proved unsuccessful.

It will be shown that the probability of losing full diversity and not meeting the coding gain specification vanishes exponentially with the Hamming distance between codewords defined as the number of different columns in pairs of codewords. Since turbo codes typically feature considerable Hamming distances, an exhaustive check of all pairs of codewords is not necessary.

Besides simplifying design, TVLT can also be used to construct full diversity space-time codes with higher rate than codes with constant modulation, e.g., 4-PSK, at each time interval. The maximum data rate limit derived in [1] for a full diversity space-time codes is based on the assumption of constant modulation. TVLT has the effect of varying the modulation at each time interval. It leads to a higher maximum rate that will be derived in this report. For example, full diversity space-time codes with 8-PSK modulation have a maximum rate of 3 b/s/Hz. A full diversity TVLT 8-PSK code with a rate of 4 b/s/Hz will be demonstrated.

Finally, it is shown that turbo STC with TVLT lend themselves to the application of a form of the *extrinsic information transfer* (EXIT) chart especially modified for the task. This method is an extension of the EXIT chart for single antenna turbo codes [13, 16, 24] to turbo STC. It provides an efficient, low complexity method to quickly predict the performance of turbo STC. With this convenient tool, different designs and different codes and can be easily compared, and the best one can be selected. Several new turbo STC are developed and analyzed in this manner.

The remainder of this chapter is organized as follows. In Section 3.1, after presenting the channel model, TVLT codes are introduced. Salient properties of turbo STC with TVLT are explored in Section 3.2. The performance analysis based on the EXIT charts is developed in Section 3.3. Numerical results are presented in Section 3.4 and concluding remarks are found in Section 3.5.

3.1 Channel Model and TVLT

In this chapter MIMO systems with n_T transmit and n_R receive antennas over block Rayleigh fading channel are considered. The received signal at time interval t is

$$\mathbf{r}(t) = \mathbf{H}\mathbf{x}(t) + \mathbf{n}(t), \tag{3.1}$$

where $\mathbf{x}(t)$ is the $n_T \times 1$ vector of the transmitted signal; $\mathbf{r}(t)$ is the $n_R \times 1$ received signal vector; $\mathbf{H}$ is the $n_R \times n_T$ channel gain matrix, which consists of complex-valued scalars $h_{ij}, i = 1, ..., n_R$, $j = 1, ..., n_T$, modeled as zero-mean, mutually independent, identically distributed Gaussian random variables with unity variance The term $\mathbf{n}(t)$ is zero-mean, additive white Gaussian noise (AWGN) with variance $n_T/(2\,\mathrm{SNR})$ per dimension, where SNR is the signal to noise ratio per symbol. With this model, the mean SNR at the receiver is independent of the number of transmit antennas.

The transmitter with TVLT is shown in Figure 3.1. Denote a codeword produced by the encoder $\mathbf{C} = [\mathbf{c}(1), ..., \mathbf{c}(L)]$, with L the codeword length. At each time interval t, $t = 1, .., L$, a vector of coded symbols $\mathbf{c}(t) = [c_1(t), ..., c_{n_T}(t)]^T$ is multiplied by a predetermined $n_T \times n_T$ unitary matrix $\mathbf{G}(t)$ and yields the vector of symbols $\mathbf{x}(t)$, which is subsequently transmitted,

$$\mathbf{x}(t) = \mathbf{G}(t)\mathbf{c}(t). \tag{3.2}$$

The set of unitary matrices $\{\mathbf{G}(t)\}_{t=1}^{L}$ is generated randomly, independent of the codewords it is applied to. Once generated, the set is stored both at the transmitter and at the receiver and it stays fixed for the duration of the communication. Insofar as the elements of $\mathbf{G}(t)$ are time-varying and realizations of random variables, $\mathbf{x}(t)$ appear to be subject to a time-varying, random modulation. At the receiver, a random modulation is considerably simpler to demodulate than to decode a random code since demapping is carried out symbol by symbol rather than on long sequences.

Next, the generation of these unitary matrices for an arbitrary number of transmit antennas is discussed. For $p, q = 1, ..., n_T$, let $g_{p,q}(t)$ be the elements, and $\mathbf{g}_q(t)$ be the columns of $\mathbf{G}(t)$. Since $\mathbf{G}(t)$ is unitary, it must satisfy

$$\mathbf{g}_p^{\dagger}(t)\mathbf{g}_q(t) = \begin{cases} 1 & p = q \\ 0 & p \neq q \end{cases}, \tag{3.3}$$

where the superscript denotes conjugate transpose. Since the elements $g_{p,q}(t)$ are generally complex-valued, then each $\mathbf{G}(t)$ is specified by $2n_T^2$ real-valued

31
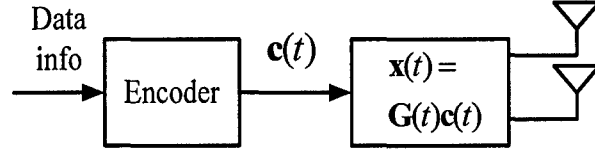
Figure 3.1: Structure of a transmitter with space-time encoder and time varying linear transformation.

parameters of which n_T^2 are prescribed by (3.3) and the rest are free, but constrained $|g_{p,q}(t)|^2 \leq ||\mathbf{g}_q(t)||^2 = 1$. These requirements can be met by elements of the following form:

$$g_{p,q}(t) = \cos \alpha_{p,q}(t) e^{j\beta_{p,q}(t)},$$

where $\alpha_{p,q}(t)$, $\beta_{p,q}(t) \in [0, 2\pi)$. Of these, n_T^2 are independent realizations picked from the uniform distribution over $[0, 2\pi)$ and the other n_T^2 terms are found from (3.3). Of particular interest in this report is the case $n_T = 2$, for which $\alpha_{11}(t)$, $\beta_{11}(t)$, $\beta_{12}(t)$, $\beta_{21}(t)$ are picked and (3.3) is solved for the rest to obtain

$$\mathbf{G}(t) = \begin{bmatrix} \cos \alpha_{11}(t) e^{j\beta_{11}(t)} & \sin \alpha_{11}(t) e^{j\beta_{12}(t)} \\ -\sin \alpha_{11}(t) e^{j\beta_{21}(t)} & \cos \alpha_{11}(t) e^{j(-\beta_{11}(t)+\beta_{12}(t)+\beta_{21}(t))} \end{bmatrix}. \qquad (3.4)$$

3.2 Turbo-STC with TVLT

In this section, properties of turbo space–time codes with TVLT are investigated. It is shown that full diversity can be practically assured. In addition, if the minimum Hamming distance between all pairs of space-time codewords is sufficiently large, the coding gain exceeds a prescribed threshold with high probability. The Hamming distance between two codewords is defined as the number of columns that are different between the codewords. Finally, the throughput rate of these codes is investigated and is shown to exceed the maximum rate for conventional space-time codes derived in [1].

32

3.2.1 Diversity and Coding Gains

Let two distinct codewords of a space-time code be represented by the $n_T \times L$ matrices $\mathbf{C} = [\mathbf{c}(1)...\mathbf{c}(L)]$ and $\mathbf{B} = [\mathbf{b}(1)...\mathbf{b}(L)]$, respectively. According to the rank criterion, the code achieves full transmit diversity if for every possible pair of codewords $\mathbf{C}$ and $\mathbf{B}$, the error matrix $\mathbf{E} = [\mathbf{e}(1), ..., \mathbf{e}(L)]$, where $\mathbf{e}(t) = \mathbf{c}(t) - \mathbf{b}(t)$, has rank n_T [1]. For special space-time codes, simple proofs of full diversity can be found [1], however, for the general case, ascertaining full diversity is a cumbersome process that requires testing the rank of all pairs of codewords. When the test fails, the encoder is redesigned and the test starts over. For turbo space-time codes, there are no explicit guidelines for designing full diversity codes. According to [8], without the tedious check-adjust process, a turbo space-time code with a randomly picked interleaver usually fails to achieve full diversity.

For a full diversity space-time code, the coding gain achieved by the pair $\mathbf{B}$, $\mathbf{C}$ is $\xi = (\lambda_1, ..., \lambda_{n_T})^{1/n_T} = \left(\det \left(\mathbf{E}\mathbf{E}^\dagger \right) \right)^{1/n_T}$, where $\lambda_1, ..., \lambda_{n_T}$ denote the n_T eigenvalues of $\mathbf{E}\mathbf{E}^\dagger$ [1]. The coding gain of the space-time code is the minimum of ξ sought over all pairs of codewords.

Consider now a space-time code with TVLT. Let two codewords be $\overline{\mathbf{B}} = [\mathbf{G}(1)\mathbf{b}(1), ..., \mathbf{G}(L)\mathbf{b}(L)]$ and $\overline{\mathbf{C}} = [\mathbf{G}(1)\mathbf{c}(1), ..., \mathbf{G}(L)\mathbf{c}(L)]$, respectively, and the corresponding error matrix $\overline{\mathbf{E}} = [\mathbf{G}(1)\mathbf{e}(1), ..., \mathbf{G}(L)\mathbf{e}(L)]$. Let d_h be the Hamming distance between $\mathbf{B}$ and $\mathbf{C}$, i.e., the number of nonzero columns in $\mathbf{E}$. It follows immediately that d_h is also the number of non-zero columns in $\overline{\mathbf{E}}$, except for the rare occasion when $\overline{\mathbf{e}}(t) = \mathbf{G}(1)\mathbf{e}(t) = \mathbf{0}$, but $\mathbf{e}(t) \neq \mathbf{0}$. Since the elements of the transformations $\{\mathbf{G}(t)\}_{t=1}^L$ are realizations of random variables, with high probability, for $d_h \geq n_T$, rank $\overline{\mathbf{E}} = n_T$, thus giving the code full diversity.

The linear transformations $\{\mathbf{G}(t)\}_{t=1}^L$ affect the diversity gain and coding gain in a manner specified by the following theorems.

Theorem 1 *Let $\mathbf{B}$ and $\mathbf{C}$ be a pair of $n_T \times L$ codewords with Hamming distance d_h. Let $d_{\max}^2$ be the largest Euclidean norm of all columns of $\mathbf{E}$, i.e., $d_{\max}^2 = \max_{t=1,...,L} \{\|\mathbf{e}(t)\|^2\}$, and $d_{\min}^2$ be the smallest norm of all nonzero columns of $\mathbf{E}$, i.e., $d_{\min}^2 = \min_{t=1,...,L} \{\|\mathbf{e}(t)\|^2, \|\mathbf{e}(t)\|^2 \neq 0\}$. With $\overline{\mathbf{B}}$, $\overline{\mathbf{C}}$ the corresponding pair of codewords following TVLT, define the error matrices $\mathbf{E} = \mathbf{C} - \mathbf{B}$ and $\overline{\mathbf{E}} = \overline{\mathbf{C}} - \overline{\mathbf{B}}$. Then $\Pr \left\{ \det \left(\overline{\mathbf{E}}\overline{\mathbf{E}}^\dagger \right) < u \right\}$, the probability that $\det \left(\overline{\mathbf{E}}\overline{\mathbf{E}}^\dagger \right)$ is lower than a given threshold u, where $0 < u < d_{\max}^2 \cdot (d_{\min}^2)^{n_T - 1}$,*

decreases exponentially with $\lfloor d_h/(n_T - 1) \rfloor$, *where* $\lfloor x \rfloor$ *denotes the largest integer less than* x.

Proof. Without loss of generality, rearrange $\mathbf{E}$ such that the nonzero columns are listed first. In particular, let the first column be the one with the largest norm $d_{\max}^2$. Then, following TVLT, we have

$$
\begin{aligned}
\overline{\mathbf{E}} &= [\mathbf{G}(1)\mathbf{e}(1), ..., \mathbf{G}(d_h)\mathbf{e}(d_h), 0, ..., 0] \\
&\triangleq [\overline{\mathbf{e}}(1), ..., \overline{\mathbf{e}}(d_h), 0, ..., 0].
\end{aligned}
$$

Divide the columns $\{\overline{\mathbf{e}}(2), ..., \overline{\mathbf{e}}(d_h)\}$ into $U = \lfloor d_h/(n_T - 1) \rfloor$ disjoint partitions, each containing $n_T - 1$ columns, and concatenate each partition with the first column of $\overline{\mathbf{E}}$ to construct U square matrices $\mathbf{V}(\mu)$, $\mu = 1, ..., U$. Each matrix $\mathbf{V}(\mu)$ is generated by a set of $(n_T - 1)$ transformations $\mathbf{G}(t)$. Since the first column is common to all $\mathbf{V}(\mu)$, its transformation can be absorbed in the MIMO channel. Recalling that each $\mathbf{G}(t)$ is obtained from n_T^2 realizations of a random variable, it follows that its domain is a hypercube with volume $(2\pi)^{n_T^2}$. Extending this reasoning to $\mathbf{V}(\mu)$, its domain is a hypercube with volume $\Psi_\mu = (2\pi)^{(n_T-1)n_T^2}$.

The determinant $\det\left(\mathbf{V}(\mu)^\dagger \mathbf{V}(\mu)\right)$ is a continuous function of the angles forming the transformations $\mathbf{G}(t)$, since its value is determined by trigonometric and exponential functions of these angles. Moreover, $\det\left(\mathbf{V}(\mu)^\dagger \mathbf{V}(\mu)\right)$ is bounded by $0 \leq \det\left(\mathbf{V}(\mu)^\dagger \mathbf{V}(\mu)\right) \leq \prod_{k=1}^{n_T} \left(\mathbf{V}(\mu)^\dagger \mathbf{V}(\mu)\right)_{kk}$, where $\left(\mathbf{V}(\mu)^\dagger \mathbf{V}(\mu)\right)_{kk}$ is an element on the diagonal of the matrix $\mathbf{V}(\mu)^\dagger \mathbf{V}(\mu)$. The left hand side of the inequality follows from the non-negative property of a determinant of a Hermitian matrix, and the right hand side is a consequence of Hadamard's inequality. Direct evaluation shows that for any μ, $\prod_{k=1}^{n_T} \left(\mathbf{V}(\mu)^\dagger \mathbf{V}(\mu)\right)_{kk} = d_{\max}^2 \prod_{t=(\mu-1)(n_T-1)+1}^{\mu(n_T-1)} ||\mathbf{e}(t)||^2$. As the TVLT transformations $\mathbf{G}(t)$ range through all possible values, $\det\left(\mathbf{V}(\mu)^\dagger \mathbf{V}(\mu)\right)$ maps onto all values between the two bounds.

Consequently, for any u, with $0 < u < d_{\max}^2 \left(d_{\min}^2\right)^{n_T-1} \leq d_{\max}^2 \prod_{t=(\mu-1)\cdot(n_T-1)+1}^{\mu\cdot(n_T-1)} ||\mathbf{e}(t)||^2$, there exists a non-empty Υ_μ region in Ψ_μ such that if the domain of $\mathbf{V}(\mu)$,

$\mathbf{A}_\mu \in \Upsilon_\mu$, then $\det\left(\mathbf{V}(\mu)^\dagger \mathbf{V}(\mu)\right) \geq u$. Let $\overline{\Upsilon}_\mu$ denote the complement region of Υ_μ, that is if $\mathbf{A}_\mu \in \overline{\Upsilon}_\mu$, then $\det\left(\mathbf{V}(\mu)^\dagger \mathbf{V}(\mu)\right) < u$. Then, if the volume of $\overline{\Upsilon}_\mu$ is denoted $|\overline{\Upsilon}_\mu|$,

$$\Pr\left\{\det(\mathbf{V}(\mu)^\dagger \mathbf{V}(\mu) < u\right\} \qquad (3.5)$$

$$= \frac{|\overline{\Upsilon}_\mu|}{(2\pi)^{(n_T-1)n_T^2}} < 1.$$

Next the inequality $\det\left(\overline{\mathbf{E}\mathbf{E}}^\dagger\right) \geq \det\left(\mathbf{V}(\mu)^\dagger \mathbf{V}(\mu)\right)$, $\mu = 1, ..., U$, is proved for later use. Since matrix $\overline{\mathbf{E}}$ incorporates $\mathbf{V}(\mu)$ and has additional columns, denoted $\phi_1, ..., \phi_{d_h-\mu}$. According to the rank-one updates theorem for determinants [25], $\det\left(\mathbf{A} + \mathbf{c}\mathbf{d}^\dagger\right) = \det\left(\mathbf{A}\right)\left(1 + \mathbf{d}^\dagger \mathbf{A}^{-1}\mathbf{c}\right)$ where $\mathbf{A}$ is $n \times n$ and $\mathbf{c}, \mathbf{d}$ are $n \times 1$. Then,

$$\det\left(\overline{\mathbf{E}\mathbf{E}}^\dagger\right) = \det\left(\mathbf{V}(\mu)\mathbf{V}(\mu)^\dagger + \sum_{i=1}^{d_h-\mu} \phi_i \phi_i^\dagger\right).$$

Apply the theorem one column at a time

$$\begin{aligned}
\det\left(\overline{\mathbf{E}\mathbf{E}}^\dagger\right) &= \det\left(\left(\mathbf{V}(\mu)\mathbf{V}(\mu)^\dagger + \sum_{i=2}^{d_h-\mu} \phi_i \phi_i^\dagger\right) + \phi_1 \phi_1^\dagger\right) \\
&= \det\left(\mathbf{V}(\mu)\mathbf{V}(\mu)^\dagger + \sum_{i=2}^{d_h-\mu} \phi_i \phi_i^\dagger\right)\left(1 + \phi_1^\dagger \phi_1\right).
\end{aligned}$$

Repeating this step for all columns, the claim is proved

$$\begin{aligned}
\det\left(\overline{\mathbf{E}\mathbf{E}}^\dagger\right) &= \det\left(\mathbf{V}(\mu)\mathbf{V}(\mu)^\dagger\right) \prod_{i=1}^{d_h-\mu}\left(1 + \phi_i \phi_i^\dagger\right) \qquad (3.6) \\
&\geq \det\left(\mathbf{V}(\mu)\mathbf{V}(\mu)^\dagger\right).
\end{aligned}$$

With the inequality (3.6) proved, it follows that,

$$\Pr\left\{\det\left(\overline{\mathbf{E}}\overline{\mathbf{E}}^{\dagger}\right) < u\right\}$$

$$\leq \Pr\left\{\det\left(\mathbf{V}(1)^{\dagger}\mathbf{V}(1)\right) < u, ..., \det\left(\mathbf{V}(U)^{\dagger}\mathbf{V}(U)\right) < u\right\}$$

$$= \prod_{\mu=1}^{U} \Pr\left\{\det\left(\mathbf{V}(\mu)^{\dagger}\mathbf{V}(\mu)\right) < u\right\}$$

$$= \prod_{\mu=1}^{U} \frac{|\overline{\Upsilon}_{\mu}|}{(2\pi)^{(n_T-1)n_T^2}}$$

$$\leq r^{\lfloor d_h/(n_T-1)\rfloor}, \tag{3.7}$$

where

$$r = \max_{\mu=1,...,U}\left\{\frac{|\overline{\Upsilon}_{\mu}|}{(2\pi)^{(n_T-1)n_T^2}}\right\}. \tag{3.8}$$

In (3.7), line 3 follows since $\{\mathbf{V}(\mu), \mu = 1, \cdots, U\}$ are independent; in line 5, recall that $U = \lfloor d_h/(n_T-1)\rfloor$. ■

The following two theorems follow directly from Theorem 1.

Theorem 2 *The probability that $\overline{\mathbf{E}}$ does not have full rank decreases to zero exponentially with $\lfloor d_h/(n_T-1)\rfloor$.*

Proof. According to Theorem 1,

$$Pr\left\{\text{rank } \overline{\mathbf{E}} < n_T\right\}$$

$$= Pr\left\{\det\left(\overline{\mathbf{E}}\overline{\mathbf{E}}^{\dagger}\right) = 0\right\}$$

$$< Pr\left\{\det\left(\overline{\mathbf{E}}\overline{\mathbf{E}}^{\dagger}\right) < u\right\},$$

where $0 < u < d_{\max}^2 \cdot (d_{\min}^2)^{n_T-1}$ is a threshold such that if $\det\left(\overline{\mathbf{E}}\overline{\mathbf{E}}^{\dagger}\right) < u$ then the matrix $\overline{\mathbf{E}}\overline{\mathbf{E}}^{\dagger}$ is claimed to lose full rank. Since $Pr\left\{\det\left(\overline{\mathbf{E}}\overline{\mathbf{E}}^{\dagger}\right) < u\right\}$ decrease to zero exponentially with $\lfloor d_h/(n_T-1)\rfloor$, then $Pr\left\{\text{rank } \overline{\mathbf{E}} < n_T\right\}$ also decrease to zero exponentially with $\lfloor d_h/(n_T-1)\rfloor$. ■

Theorem 3 *Let the coding gain achieved by the pair of codewords $\overline{\mathbf{B}}$, $\overline{\mathbf{C}}$ be $\xi = \left(\det\left(\overline{\mathbf{E}}\,\overline{\mathbf{E}}^{\dagger}\right)\right)^{1/n_T}$, where $\overline{\mathbf{E}} = \overline{\mathbf{B}} - \overline{\mathbf{C}}$. Then $Pr\{\xi < w\}$, the probability that the coding gain is less than a threshold w, where $0 < w < \left(d_{\max}^2 \cdot (d_{\min}^2)^{n_T - 1}\right)^{1/n_T}$ decreases to zero exponentially with $\lfloor d_h/(n_T - 1)\rfloor$.*

Proof.

$$\Pr\{\xi < w\}$$
$$= \Pr\{\xi^{n_T} < w^{n_T}\}$$
$$= \Pr\left\{\det\left(\overline{\mathbf{E}}\,\overline{\mathbf{E}}^{\dagger}\right) < u\right\},$$

where $0 < u \triangleq w^{n_T} < d_{\max}^2 \cdot (d_{\min}^2)^{n_T - 1}$. Then according to Theorem 1, $\Pr\{\xi < w\}$ decreases to zero exponentially with $\lfloor d_h/(n_T - 1)\rfloor$. ■

Theorem 1, 2, and 3 answer the question: what is the probability that the code lose diversity and the coding gain falls below a set value. These theorems state that both probability vanish exponentially with the ratio $\lfloor d_h/(n_T - 1)\rfloor$. It follows that a desired feature of space-time codes with TVLT is a large Hamming distance. If for all pairs of codewords the minimum Hamming distance is large then the space-time code achieves full diversity and good coding gain with a high probability.

As to the question how large $d_{h,\min}$ should be, there is no general answer. An example is provided below to demonstrate the theorems.

Example 1. Consider the design of a full diversity TVLT space-time code for $n_T = 2$ and 4-PSK modulation. We want to show how large the Hamming distance $d_{h,\min}$ should be to guarantee that the probability of full diversity is not achieved and the coding gain falling below a specified value is very small.

Say that $\Pr\left\{\det\left(\overline{\mathbf{E}}\,\overline{\mathbf{E}}^{\dagger}\right) < u\right\} < 10^{-6}$ is required for some u. According to (3.7), if r can be found, then the required d_h can be determined. In this example, with $n_T = 2$, $\mathbf{V}(\mu)$ in (3.5) has only two columns

$$\mathbf{V}(\mu) = [\mathbf{e}(1), \mathbf{G}(\mu)\,\mathbf{e}(\mu)],$$

where without loss of generality it was assumed that $\mathbf{G}(1)$ is the identity matrix (one transformation can always be factored out of the codeword and can be made part of the channel). Let two pairs of transmitted two-tuple symbols with differences $\mathbf{e}(1)$ and $\mathbf{e}(\mu)$, respectively. Also let $\mathbf{G}(\mu)$ be given in

37

(3.4) and its four angles taking values on a grid in $[0, 2\pi)$ with spacings $\pi/50$. For the given symbols and for each $\mathbf{G}(\mu)$, we calculate $\det\left(\mathbf{V}(\mu)^\dagger \mathbf{V}(\mu)\right)$. We count the number of realizations of $\mathbf{G}(\mu)$ that make $\det\left(\mathbf{V}(\mu)^\dagger \mathbf{V}(\mu)\right) < u^2$, and denote that number $K(m, \mu, u)$, where m indexes the pairs of two-tuples and μ indexes the partition. Then the value $|\overline{\Upsilon}_\mu|$ in (3.5) can be approximated by this K. We have

$$\frac{|\overline{\Upsilon}_\mu|}{(2\pi)^{(r-1)\cdot n_T^2}} \approx \frac{K(m, \mu, u)}{100^4}$$

Checking over all pairs of symbols and noting the largest count for which the coding gain fails the threshold, we have

$$K(\mu, u) = \max_m \left\{ K(m, \mu, u) \right\}$$

Next, the largest value of $K(\mu, u)$ is found over all partitions μ for the given code. Let

$$K(u) = \max_\mu \left\{ K(\mu, u) \right\},$$

then from (3.8), we have

$$
\begin{aligned}
r &= \max_{\mu = 1, \ldots, U} \left\{ \frac{|\overline{\Upsilon}_\mu|}{(2\pi)^{(M-1)M^2}} \right\} \\
&\approx \max_{\mu = 1, \ldots, U} \left\{ \frac{K(\mu, u)}{100^4} \right\} \\
&= \frac{K(u)}{100^4}.
\end{aligned}
$$

Assume a threshold of $u = d_{\min}^2/8 = E_s/4$, where E_s is the energy of a 4-PSK symbol, is set such that if $\det\left(\overline{\mathbf{EE}^\dagger}\right) > u$ then $\overline{\mathbf{EE}^\dagger}$ is ensured to be full rank. It is found that $r \approx 0.0462$. It follows that a code with a Hamming distance of $d_{h,\min} = 5$ makes $\Pr\left\{ \det\left(\overline{\mathbf{EE}^\dagger}\right) < E_s/4 \right\} \approx 2 \times 10^{-7} < 10^{-6}$. In another example, if $u = (d_{\min}^2)^2/2 = (E_s)^2$, or a coding gain threshold of E_s is required, it is found that $r \approx 0.27$, and $d_{h,\min} = 11$ is required for $\Pr\left\{ w < E_s \right\} < 10^{-6}$. ∎

Conventional space-time trellis codes, such as proposed in [1], generally do not satisfy a large Hamming distance requirement. That means that

application of TVLT to such codes could potentially result in low coding gain. Hence, TVLT is not suitable to be used with conventional space-time trellis codes.

Although not much is known about efficient methods to calculate the minimum Hamming distances for arbitrary, non-binary turbo space-time codes, such codes usually feature relatively large minimum Hamming distances. Even when there are low weight codewords (leading to low Hamming distances), their number is small and they do not have a significant impact on performance [26]. The calculation of $d_{h,\min}$ for binary turbo codes is better known. For example, in [27] it is shown that for a rate 1/2, eight-state binary turbo code with convolutional component codes and interleaver size 1000, the upper bound on the minimum Hamming distance is about 100.

Hence, Theorem 1, 2, 3 and example 1 suggest that with TVLT, full diversity as well as good coding gain of turbo space-time codes can be virtually ensured.

3.2.2 Rate

According to Theorem 3.3.1 and Corollary 3.3.1 in [1], for a n_T transmit and n_R receive antennas, and signal constellation size 2^b, the full diversity of $n_T n_R$ can be achieved with a maximum rate of b bits/s/Hz. Inspection of the proof in the reference, reveals that the rate limit is a consequence of the restriction of constant modulation during the codeword. With TVLT, this restriction is removed, since the modulation constellation changes each time interval. Consequently, a new rate derivation is required for space-time codes with TVLT.

The next theorem completes the characterization of space-time codes with TVLT, by establishing the code rate and its relation to the Hamming distance.

Theorem 4 *Consider a space-time code for n_T transmit antennas. Assume a signal constellation $\mathcal{Q}$ (before TVLT application) with cardinality $|\mathcal{Q}| = 2^b$ elements. Let L denote the codeword length. Then the maximum rate of a code with minimum Hamming distance $d_{h,\min}$ is*

$$R \leq n_T b - \frac{1}{L} \log_2 V,$$

39

in bits per channel use, where

$$V = \sum_{j=0}^{d_{h,\min}} \binom{L}{j} \left(2^{n_T b} - 1\right)^j .$$

Proof. Regard the columns of the $n_T \times L$ space-time codeword matrix as supersymbols defined over a superalphabet constellation $\mathcal{Q}^{n_T}$ with $|\mathcal{Q}^{n_T}| = 2^{n_T b}$. Each codeword can be viewed as an L-tuple in a L-dimensional space $[\mathcal{Q}^{n_T}]^L$. The sphere-packing bound [28] can be applied to obtain the maximum rate. Imagine a ball of radius $d_{h,\min}$ in the L-dimensional space, centered at a codeword point, including all points at Hamming distances $0, 1, ..., d_{h,\min}$. The number of such points is given by [28]

$$V = \sum_{j=0}^{d_{h,\min}} \binom{L}{j} \left(2^{n_T b} - 1\right)^j .$$

Associate one such ball with each codeword. The total number of L-tuples is $(2^{n_T b})^L$. Then the maximum number of valid codewords separated by at least $d_{h,\min}$ is

$$A = \frac{(2^{n_T b})^L}{V}.$$

Hence the maximum transmission rate rate is

$$\begin{aligned} R &\leq \frac{1}{L} \log_2 A \\ &= n_T b - \frac{1}{L} \log_2 V. \end{aligned}$$

∎

Example Assume a turbo-STC with $n_T = 2$, $L = 1024$, $b = 3$ (8-PSK modulation), and $d_{h,\min} = 12$. Then according to Theorem 4, the maximum rate is 5.84 bits/channel use, which for PSK corresponds to the same number of bits/sec/Hz. According to [1], with constant modulation, the maximum rate for a full diversity code is 3 b/s/Hz. Later in this chapter, a rate 4 b/s/Hz code with 8PSK modulation that achieves full diversity is demonstrated.∎ .

This section on turbo-STC with TVLT is concluded with a brief discussion on implementation complexity. At the transmitter, one extra matrix multiplication is needed at every symbol interval. The added complexity is not significant, especially when the number of transmit antennas is two. Also at the receiver, an extra matrix multiplication is required for every symbol interval when compared to codes without TVLT.

3.3 Design and Convergence Analysis

Conventional space time codes with full diversity and high coding gain have to be either hand designed [1] or found by exhaustive search [10]. This approach is very inefficient for turbo-STC, since two optimal component encoders do not necessarily guarantee a good overall turbo code, and the search also has to include the random interleaver. In the previous section, it has been shown that turbo-STC with TVLT has full diversity and also a high probability of coding gain. This serves as a good starting point in the design of turbo-STC, but an analysis tool for these codes is also needed to facilitate "tweaking" the design. Such a tool exists for binary [13], non-binary [16], and coded modulation [24], in the form of the EXIT chart. Here, the EXIT chart method is extended to the turbo space-time code with TVLT and is used to predict the convergence behavior of the turbo decoder. This extension greatly expedites the code design process.

It will be shown that with TVLT, the code performance depends on the n_T singular values of the channel matrix $\mathbf{H}$ rather than the channel matrix itself. In the rest of the chapter, codes for two transmit antennas are exclusively considered. For this case, it will be shown that with $n_T = 2$, the EXIT chart can be applied to find the convergence region defined on the 2-D plane of the channel singular values. Finally, the method by which the chart can be applied to predict the code performance is presented.

3.3.1 Encoder

Generally speaking, space-time codes are multidimensional codes [17,29] with the additional constraint of the rank criterion. With TVLT, full diversity is guaranteed without appealing to the rank criterion. The turbo-STC is designed using accepted design practice for turbo codes. In Figure 3.2, is shown the general structure of a turbo space-time code encoder with TVLT. The component encoders are two identical, recursive, systematic convolutional (RSC) encoders. The output parity bits of the two RSCs are alternatively punctured. The mapping from the coded bits to symbols is the 4-D set partition proposed in [29].

Several new turbo codes are introduced in this report for which the component encoders are listed in Table 3.1. The notation used in the table and Figure 3.2 follows [17]. The quantities m and v denote the number of input information bits and the constraint length, respectively. Each cir-

cle in Figure 3.2 represents a switch. The binary variable next to each switch, $\{h_i^j,\ i = 1, ...v,\ j = 0, ...m\}$ or $\{f^k,\ k = 1, ..., v\}$, indicates whether the switch is in the "on" position. For compact representation, the polynomial notation $H^j(D)$ is used to indicate the connections of the input bit j to the mod 2 adders of the convolutional code,

$$H^j(D) = \sum_{i=1}^{v} h_i^j D^i.$$

The feedback is represented by $H^0(D)$ and the feedforward by $F(D)$,

$$F(D) = \sum_{k=1}^{v} f^k(D).$$

All numbers shown in the table are octal. For example, for Code 3, the $H^3(D)$ coefficients are $(04)_8 = (001000)_2$. Then

$$H^3(D) = 1 \cdot D^3 + 0 \cdot D^2 + 0 \cdot D^1 + 0 \cdot D^0,$$

or, $h_1^3 = 0$, $h_2^3 = 0$, $h_3^3 = 0$, and $h_4^3 = 1$.

Table 3.1: List of encoders used in this report, with rates 2, 3, 4 b/s/Hz, respectively

Code	m	v	$H^0(D)$	$H^1(D)$	$H^2(D)$	$H^3(D)$	$H^4(D)$	$F(D)$
(1)	2	3	6_8	1_8	2_8			3_8
(2)	3	4	10_8	01_8	02_8	04_8		07_8
(3)	4	4	10_8	01_8	02_8	04_8	10_8	03_8

3.3.2 Decoder

The structure of the turbo space-time decoder is shown in Figure 3.3. It is based on [7] and [11]. It consists of two MAP decoders, which exchange
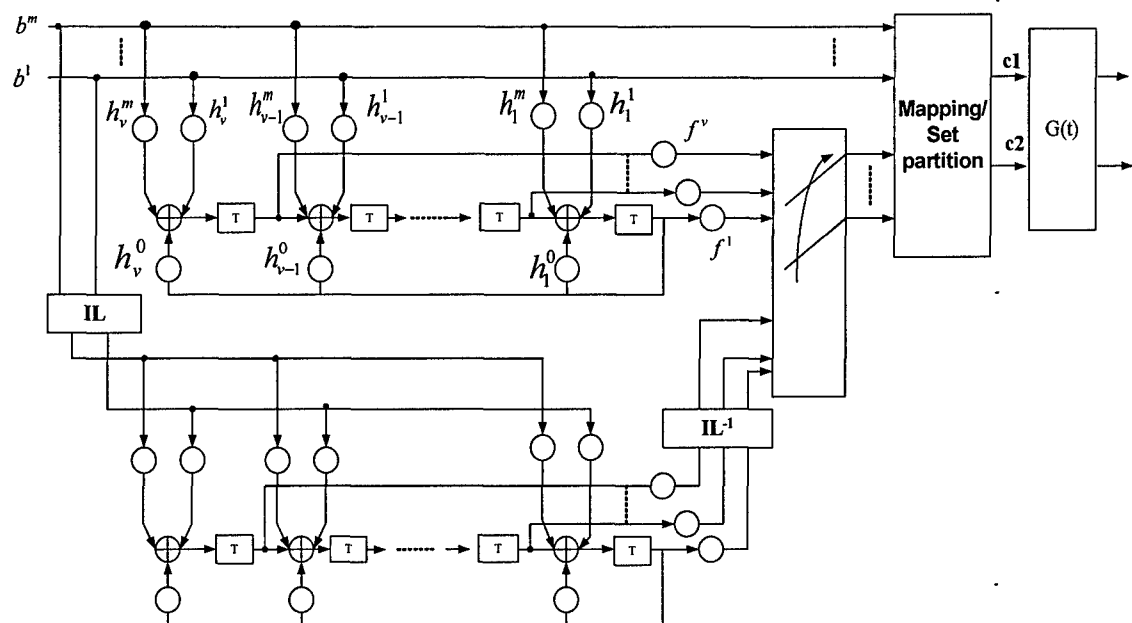
Figure 3.2: Recursive, systematic, convolutional component encoder for turbo-STC.

extrinsic information. The major difference with the binary turbo decoder is that the information passed from one component decoder to another may be a mixture of extrinsic and systematic information, as shown next. In binary turbo decoders, the information exchanged between component decoders contains only extrinsic information.

Let $\mathbf{L}_p$ and $\mathbf{L}_a$ denote respectively, the *a posteriori* and *a priori* information in log-likelihood form. Consider any one of the component decoders. Then there are two possible cases: (i) at time t the parity bits from the corresponding component encoder are transmitted; (ii) at time interval t the parity bits from the encoder are punctured. Then the *a posteriori* information can be expressed

$$\mathbf{L}_p\left(t\right) = \left\{ \begin{array}{ll} \mathbf{L}_a\left(t\right) + \mathbf{L}_{es}\left(t\right), & \text{(i)} \\ \mathbf{L}_a\left(t\right) + \mathbf{L}_e\left(t\right), & \text{(ii)} \end{array} \right. , \tag{3.9}$$

where $\mathbf{L}_e\left(t\right)$ denotes the extrinsic information and $\mathbf{L}_{es}\left(t\right)$ denote the mixture of extrinsic and systematic (intrinsic) information. The expression for the *a priori* information is:

$$\mathbf{L}_a\left(t\right) = \left\{ \begin{array}{ll} \mathbf{L}_{es}\left(t\right), & \text{(ii)} \\ \mathbf{L}_e\left(t\right), & \text{(i)} \end{array} \right. . \tag{3.10}$$

For more details, see the reference above. These differences with binary turbo decoder lead to differences in the generation of the EXIT charts for turbo-STC as discussed in Section 3.3.4.

3.3.3 TVLT Channel

In this subsection, the effect of TVLT on the channel model (3.1) is discussed. The singular value decomposition (SVD) of the channel gain matrix $\mathbf{H}$ is $\mathbf{H} = \mathbf{U}\boldsymbol{\Sigma}\mathbf{W}^\dagger$, where $\mathbf{U}$ is unitary $n_T \times n_T$ and for, $n_T = 2$, $\mathbf{W}$ is unitary 2×2. The diagonal matrix $\boldsymbol{\Sigma}$ contains the singular values of $\mathbf{H}$. With that, the channel model (3.1) becomes

$$\mathbf{r}(t) = \mathbf{U}\boldsymbol{\Sigma}\mathbf{W}^\dagger\mathbf{G}(t)\mathbf{c}(t) + \mathbf{n}(t) \tag{3.11}$$

or

$$\mathbf{U}^\dagger\mathbf{r}(t) = \boldsymbol{\Sigma}\mathbf{W}^\dagger\mathbf{G}(t)\mathbf{c}(t) + \mathbf{U}^\dagger\mathbf{n}(t). \tag{3.12}$$

Denote $\mathbf{y}(t) = \mathbf{U}^\dagger\mathbf{r}(t)$, and $\mathbf{Q}(t) = \mathbf{W}^\dagger\mathbf{G}(t)$, with $\mathbf{Q}(t)$ a random unitary matrix that changes each time interval. Also, let the noise term $\boldsymbol{\eta}(t) =$

44

$\mathbf{U}^\dagger \mathbf{n}(t)$. Then the equivalent channel channel model is

$$\mathbf{y}(t) = \boldsymbol{\Sigma} \mathbf{Q}(t)\mathbf{c}(t) + \boldsymbol{\eta}(t). \tag{3.13}$$

Since $\mathbf{Q}(t)$ changes randomly, the equivalent channel model is a "forced fast fading" channel. When the transmitted codeword is infinitely long, it will experience all possible values of $\mathbf{Q}(t)$. Consequently, the channel state is parameterized only by $\boldsymbol{\Sigma}$, or equivalently by the two singular values σ_1 and σ_2. If the codeword is long enough, the performance of a code will be invariant over different channels, which have the same singular values.

By applying TVLT, the number of parameters needed to characterize a $2 \times n_R$ channel has been reduced to one or two real numbers. In contrast, without TVLT, the channel is described by $2N$ complex numbers. This reduction makes it practical to apply the EXIT chart to the analysis of turbo-STC as shown next.

3.3.4 EXIT Chart

The EXIT chart method [13–16] is a convenient, low complexity tool used to analyze the convergence of iterative decoding and to predict performance of turbo codes. The turbo decoder consists of two component maximum *a posteriori* (MAP) decoders, which exchange extrinsic information as the iteration proceeds. Convergence to the correct decisions depends on whether each component decoder can generate better extrinsic information than it receives from the other decoder. One assumption of this method is that the codeword length or interleaver size are long enough such that the extrinsic information log-likelihood ratios (LLRs) for different time intervals are independent [13].

The EXIT chart is a graphical representation of the input/output relation of a decoder obtained through simulations. Since usually the two component decoders are the same, only one decoder needs to be tested. To perform the test, one needs to feed the component decoder with the *a priori* LLRs of the transmitted data symbols as if they were passed from the other decoder. The decoder is also fed with channel observations, generated according to a given channel model $\mathcal{H}$ and SNR. The decoder is run and the extrinsic information is measured at its output. The EXIT chart is then the plot of the function

$$I_{out} = f(I_{in}, \mathcal{H}, \text{SNR}), \tag{3.14}$$

45

where I_{in} is the mutual information between the transmitted data symbol and the *a priori* information (in LLR form), and I_{out} is the mutual information between the transmitted data and the output extrinsic information (also in LLR form).

The most important application of the EXIT chart method is to predict the performance of turbo codes. For a single antenna AWGN channel, $\mathcal{H}$ can be described by a unit gain. Then the EXIT chart is the plot of the function

$$I_{out} = f(I_{in}, \text{SNR}). \tag{3.15}$$

For a given SNR, tests for different I_{in} can be done. And if it is found that

$$I_{out} > I_{in}, \ \forall I_{in} \geq 0, \tag{3.16}$$

then the decoder will converge to correct decisions with high probability. Otherwise, the decoding will fail. It has been shown in [13] that I_{out} is a nondecreasing function of SNR. By generating the EXIT charts (3.15) for increasing SNR values, a threshold SNR_{th} can be found such that if SNR $> \text{SNR}_{th}$ then (3.16) holds, and the decoder converges. The usefulness of SNR_{th} is to predict the beginning of the waterfall region of the bit error rate (BER).

For a single input single output (SISO), block fading channel, the channel $\mathcal{H}$ can be modeled by a complex scalar h that follows some distribution and changes independently between codewords. The EXIT chart is the plot of the function

$$I_{out} = f(I_{in}, |h|^2 \text{SNR}).$$

The threshold SNR_{th} found from the EXIT chart in the AWGN channel can be used to predict the frame error rate (FER) over the block fading channel. The convergence region for the SISO, block fading channel is $\left\{ h \mid |h|^2 > \text{SNR}_{th}/\text{SNR} \right\}$. The the frame error rate is the probability that the channel gain falls into the region where the decoding fails to converge,

$$\text{FER} = \Pr\left\{ |h|^2 < \frac{\text{SNR}_{th}}{\text{SNR}} \right\}.$$

For an $n_T \times n_R$ MIMO, block fading channel , the EXIT chart is the plot of

$$I_{out} = f(I_{in}, \mathbf{H}^\dagger \mathbf{H} \, \text{SNR}).$$

46

Since $\mathbf{H}$ is constituted from $2 \times n_T \times n_R$ real numbers, the region of convergence has to be defined in a $2 \times n_T \times n_R$-dimensional space. Even for $n_T = 2$, $n_R = 1$, searching the threshold boundary of a four-dimensional space is impractical. This fact impeded the development of EXIT charts for turbo space-time codes. As explained in Section 3.3.3, application of TVLT solves this problem. The MIMO block fading channel is transformed into an equivalent forced, fast fading channel, which can be parameterized by the eigenvalues of $\mathbf{H}^\dagger \mathbf{H}\,\mathrm{SNR}$ (or the singular values of the channel gain matrix $\mathbf{H}$). For $n_T = 2$, there are at most two eigenvalues. That is, the EXIT chart is the plot of the function

$$I_{out} = f(I_{in}, \lambda_1, \lambda_2),$$

where $\lambda_{1,2}$ are the eigenvalues of $\mathbf{H}^\dagger \mathbf{H}\,\mathrm{SNR}$. The EXIT chart will be used to find the region of convergence on the 2-D plane defined by the two eigenvalues. The values that lie outside the region of convergence can be used to predict the FER performance of turbo space-time codes with TVLT. Examples will be shown in section 3.3.5.

To generate the EXIT chart for turbo-STC with TVLT, an approach similar to the one proposed in Chapter 2 for SISO turbo trellis coded modulation is taken. The input to the component MAP decoder is either generated as pure extrinsic information or is synthesized as a mixture of extrinsic and systematic information, according to (3.10). Also, the output of the component MAP decoder is either pure extrinsic information or mixture of extrinsic and systematic information according to (3.9). In the latter case, the systematic information needs to be removed before the extrinsic information is measured. The synthesis and separation of extrinsic information and systematic information are the major differences between EXIT charts for binary and space-time turbo codes. The details of generating EXIT chart for multidimensional turbo coded modulation is found in Chapter 2.

Figure 3.4 provides examples of EXIT charts of turbo-STC with TVLT for three fixed and different channel realizations, but with the same pair of channel eigenvalues, $\lambda_1 = 1.5$, $\lambda_2 = 1.0$. The code represented is Code 1 in Table 3.1. In this figure, I_{in} and I_{out}, measured in bits-per-channel-use, label the abscissa and ordinate, respectively. The three curves are plots of $I_{out} = f(I_{in}, \mathbf{H})$ parameterized by the channel realizations. Since each transmission includes two information bits, I_{in} and I_{out} are in the range [0,2] bits. From the figure it can be seen that the three EXIT curves almost overlap with each other.
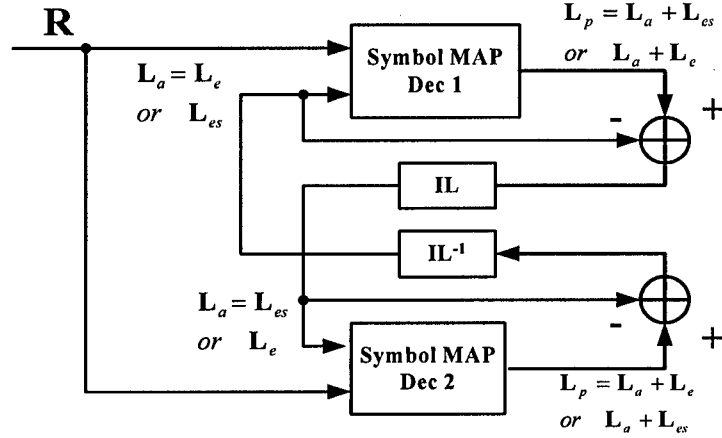
Figure 3.3: Structure of the turbo space-time decoder with two component MAP decoders.
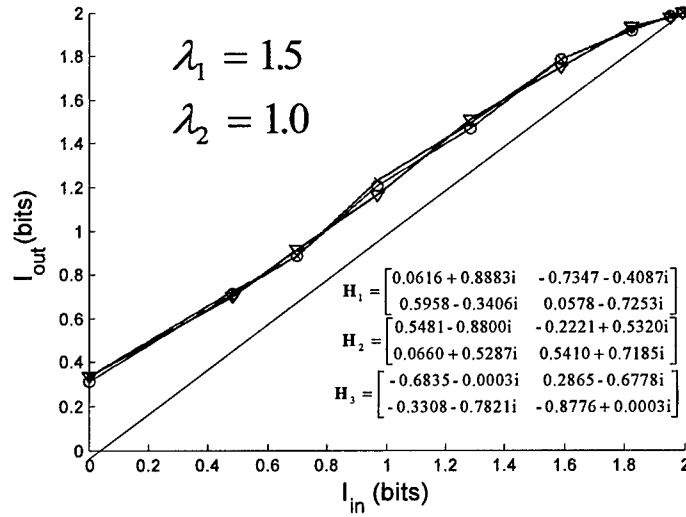

Figure 3.4: Demonstration: turbo-STC has same convergence behavior over different channels with the same eigenvalues.

48

3.3.5 Performance Analysis

The EXIT chart is generated to analyze the convergence of turbo-STC with TVLT and to evaluate the FER performance over fading channel.

Convergence Analysis.

For the convergence analysis the following theorem is needed, based on the optimality of the constituent MAP decoders.

Theorem 5 *Let I_{out} denote the mutual information between the transmitted data symbol and the output extrinsic information from a MAP decoder. Also let I_{in} denote the mutual information between the transmitted data symbol and the input a priori information to the MAP decoder. Consider the channel model (3.11) with $n_T = 2$ and $\Sigma = \text{diag}(\sqrt{\lambda_1}, \sqrt{\lambda_2})$, where $\text{diag}\,(\cdot)$ denotes a diagonal matrix. Then $I_{out} = f(I_{in}, \lambda_1, \lambda_2)$ is a nondecreasing function of both λ_1 and λ_2.*

Proof. The channel model (3.11) can be regarded as an equivalent AWGN channel with symbols transformed by $\mathbf{U\Sigma W}^\dagger\mathbf{G}(t)$. It will be shown first that in this AWGN channel, the Euclidean distance between symbols is an increasing function of the eigenvalues λ_1, λ_2. Without loss of generality, consider a scenario in which only λ_1 has been increased to $\lambda_1 + \Delta$, $\Delta > 0$. Let $d^2\,(\lambda_1, \lambda_2)$ and $d^2\,(\lambda_1 + \Delta, \lambda_2)$ denote the respective Euclidean distances. Then for $\forall\,\mathbf{U}$, $\mathbf{W}$, $\mathbf{c}_1(t)$, $\mathbf{c}_2(t)$, λ_1, and λ_2,

$$
\begin{aligned}
d^2\,(\lambda_1 + \Delta, \lambda_2) &\triangleq \left\| \mathbf{U}\,\text{diag}\left(\sqrt{\lambda_1 + \Delta}, \sqrt{\lambda_2}\right)\mathbf{W}^\dagger\mathbf{G}(t)\,(\mathbf{c}_1(t) - \mathbf{c}_2(t)) \right\|^2 \\
&= \left\| \mathbf{U}\,\text{diag}\left(\sqrt{\lambda_1}, \sqrt{\lambda_2}\right)\mathbf{W}^\dagger\mathbf{G}(t)\,(\mathbf{c}_1(t) - \mathbf{c}_2(t)) \right\|^2 \\
&\quad + \left\| \mathbf{U}\,\text{diag}\left(\sqrt{\Delta}, 0\right)\mathbf{W}^\dagger\mathbf{G}(t)\,(\mathbf{c}_1(t) - \mathbf{c}_2(t)) \right\|^2 \\
&> \left\| \mathbf{U\Sigma}_1\mathbf{W}^\dagger\mathbf{G}(t)\,(\mathbf{c}_1(t) - \mathbf{c}_2(t)) \right\|^2 \\
&= d^2\,(\lambda_1, \lambda_2)\,.
\end{aligned}
$$

For the scenario with the higher eigenvalue, the MAP decoder produces the lower bit error rate (BER). If a smaller eigenvalue was needed for increasing the mutual information, then the two scenarios can be made equivalent by injecting noise to match the increase in Euclidean distance. The injected

49
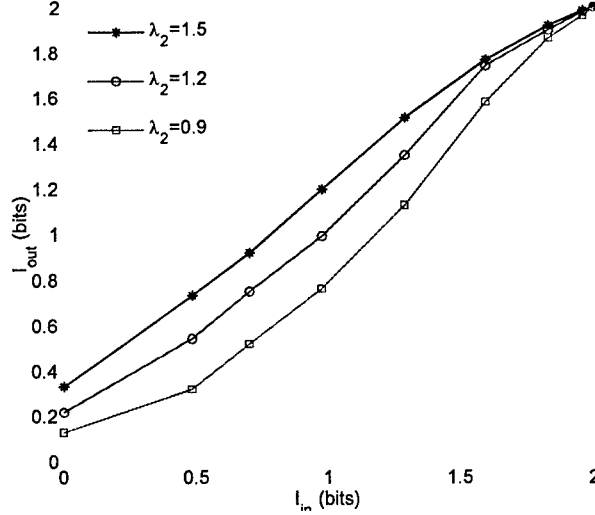
Figure 3.5: The EXIT charts of the 2 b/s/Hz code for eigenvalues $\lambda_1 = 1$ and $\lambda_2 = 0.9$, 1.2, 1.5.

noise would, however, increase the BER, which contradicts the optimality of the MAP decoder. Thus, MAP optimality dictates that the extrinsic information is non-decreasing with the eigenvalues. ■

Hence, given a λ_1, there is a minimum λ_2, denoted $\lambda_{2,min}(\lambda_1)$, such that if $\lambda_2 > \lambda_{2,min}(\lambda_1)$, then $I_{out} > I_{in}$, $\forall I_{in} \geq 0$, which guarantees the convergence of the decoder. The value $\lambda_{2,min}(\lambda_1)$ is found by gradually increasing λ_2 from a small value, until I_{out} climbs above the diagonal line. An example for Code 1 is shown in Figure 3.5. For $\lambda_1 = 1$, $\lambda_{2,min}(1)$ is found to be 1.2. Repeating the process of setting the value of λ_1 and evaluating $\lambda_{2,min}(\lambda_1)$ by the EXIT chart, results in a λ_1-λ_2 characteristic. In Figure 3.6, there are shown λ_1-λ_2 characteristics of the three codes listed in Table 3.1. The codes have rates of 2, 3, and 4 b/s/Hz, respectively. For each code, the area above the curve is the region of convergence. The higher the data rate of a code, the smaller the convergence region. In addition to displaying the region of convergence, the λ_1-λ_2 characteristic provides a convenient way to compare and select turbo space-time codes with TVLT, by quickly predicting the FER performance of the different codes, as shown in the next subsection.
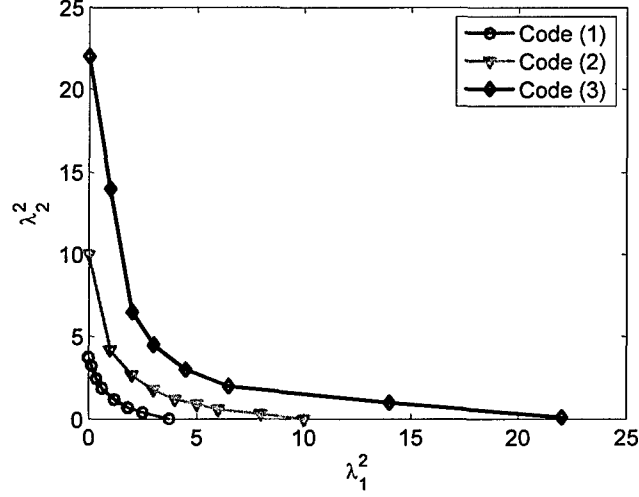
Figure 3.6: Convergence regions of the proposed codes with rate 2, 3, 4 b/s/Hz, respectively.

FER Analysis.

The λ_1-λ_2 characteristics described previously are applied to evaluate the FER of turbo-STC with TVLT. For a $2 \times n_R$ Rayleigh fading channel, where $n_R \geq 2$, the joint distribution of the eigenvalues of $\mathbf{H}^\dagger\mathbf{H}$ SNR is given by [30]

$$p(\lambda_1, \lambda_2) = \frac{1}{2\,\mathrm{SNR}^2} \exp\left(-\frac{1}{\mathrm{SNR}^3} \left(\lambda_1 + \lambda_2\right)\left(\lambda_1 - \lambda_2\right)^2 \right). \qquad (3.17)$$

Denote the region of non-convergence Γ. The FER of the code at a given signal to noise ratio SNR is the integration of $p(\lambda_1, \lambda_2)$ over the region of non-convergence such as shown in Figure 3.6. That is,

$$\mathrm{FER} = \iint\limits_{\Gamma} p(\lambda_1, \lambda_2) d\lambda_1 d\lambda_2. \qquad (3.18)$$

The integration in (3.18) can be solved either analytically or numerically. The accuracy of (3.18) will be demonstrated in the next section by comparison to simulation results.

51

An analytical expression of the FER can be found for the 2×1 channel. In this case, $\mathbf{H}^\dagger \mathbf{H}\,\mathrm{SNR}$ has a single eigenvalue. Let $\mathbf{H} = [h_1 \ h_2]^T$, then $\lambda = (|h_1|^2 + |h_2|^2)\,\mathrm{SNR}$. For Rayleigh fading, the eigenvalue λ follows a chi-square distribution with four degrees of freedom

$$p(\lambda) = \frac{1}{2\,\mathrm{SNR}^2}\lambda e^{-\lambda/\mathrm{SNR}}. \tag{3.19}$$

The minimum value of λ for which the code converges is the point $(0, \lambda_{2,\mathrm{min}})$ in Figure 3.6. This value is denoted as λ_{th}, and from the figure find for Code 1, $\lambda_{th} \simeq 3.8$. Then the FER is expressed as

$$\begin{aligned}
\mathrm{FER} &= \int_0^{\lambda_{th}} p(\lambda)d\lambda \tag{3.20} \\
&= \int_0^{\lambda_{th}} \frac{4}{\gamma^2}\lambda^2 \exp\left(-\frac{2\lambda^2}{\gamma}\right) d\lambda^2 \\
&= 1 - \left(\frac{\lambda_{th}}{\mathrm{SNR}} + 1\right)\exp\left(-\frac{\lambda_{th}}{\mathrm{SNR}}\right).
\end{aligned}$$

3.4 Numerical Results

In this section, numerical results are provided for the new codes with TVLT (Table 3.1) and their performance is compared to the case in which no TVLT is applied. The interleaver length is 1024 for all codes. The performance is measured in terms of the FER versus the SNR.

The performance of Code 1, with a spectral efficiency of 2 b/s/Hz with 4-PSK modulation, is shown in Figure 3.7, for both 2×1 and 2×2 configurations and with and without TVLT. It is observed that with TVLT, the code has a steeper FER decline with SNR, and both 2×1 and 2×2 configurations are visually parallel with the outage probability curves. Without TVLT, the codes display a marked loss in diversity gain in both configurations. The turbo-STC with TVLT gap to outage capacity is about 1-1.5 dB. This example demonstrates the ability of TVLT to provide full diversity gains (as discussed in earlier sections). The FER curve obtained from the λ_1-λ_2 characteristic is also shown in the figure. It is observed that the prediction fits the simulation sufficiently well that can be used as a quick tool to evaluate performance of turbo space-time codes.

The performance of the 8-PSK, 3 b/s/Hz Code 2 is presented in Figure 3.8 for cases similar to those in Figure 3.7. It is observed that Code 2 loses

diversity gain in the absence of TVLT, but the loss is not as marked as in the case of Code 1. A possible explanation is that the 8-PSK modulation here achieves a better rank of the error matrix than the 4-PSK modulation of Code 1. In fact, this observation reinforces the argument for TVLT, which achieves the rank criterion through diversity of the modulation. Back to the figure, it is observed that the FER predicted from the EXIT chart is reasonably close match with the simulation results.

The last in the series of performance analyses is that of Code 3 displayed in Figure 3.9. This code achieves a spectral efficiency of 4 b/s/Hz with 8-PSK modulation. As such, it breaks the rate limit of full diversity space-time codes with fixed modulation, which for 8-PSK is 3 b/s/Hz [1]. Conversely, codes at 4 b/s/Hz cannot achieve full diversity. This is clearly evident for the code without TVLT in Figure 3.9. With TVLT, however, full diversity is regained, as predicted by *Theorem 4* in Section 3.2. The EXIT chart predicts performance within 1 dB of the simulation results.
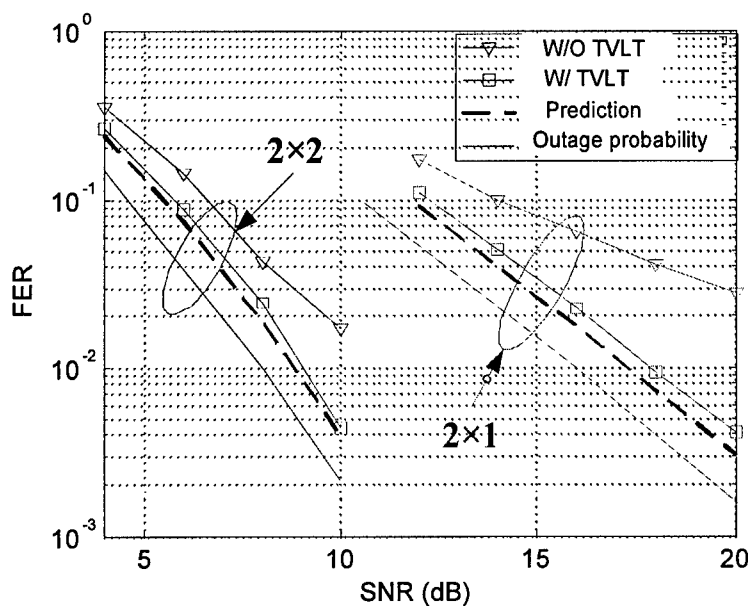

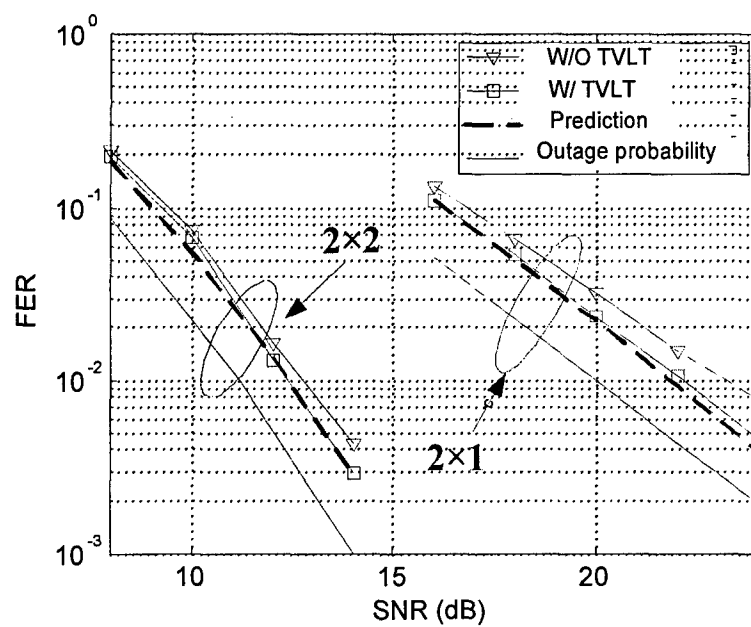Figure 3.7: FER performance comparison of the 2 b/s/Hz Code 1 with and without TVLT.

Figure 3.8: FER performance comparison of the 3 b/s/Hz Code 2 with and without TVLT.
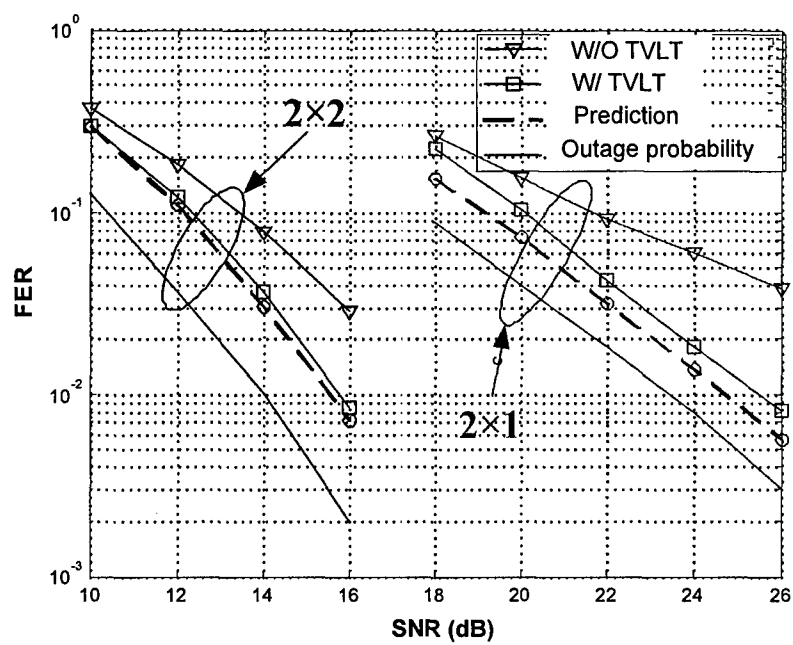
Figure 3.9: FER performance comparison of the 4 b/s/Hz Code 3 with and without TVLT.

3.5 Chapter Summary

In this chapter, time-varying linear transformations are applied to designing full diversity turbo space-time codes. TVLT consists of a unitary transformation which converts conventional, constant modulations into time varying modulations practically making the rank criterion satisfied. Unlike space-time and turbo space-time codes with fixed modulations, which may required exhaustive rank tests to ensure full diversity, the rank property is inherent to TVLT codes. Rules for the construction of TVLT have been provided for an arbitrary number of antennas. It is proved in a set of theorems that the probability that full diversity is not achieved as well as the probability that the coding gain fails to meet a prescribed level decrease exponentially with the minimum Hamming distance of the code. These theorems have two implications: (1) that the design criterion for turbo-STC is the Hamming distance between codewords (before TVLT application); (2) since turbo-STC typically display high minimum Hamming distance, they are good candidates for use with TVLT. A second theorem established the rates achievable with TVLT space-time codes. It was shown that limits due to constant modulation over the codeword duration do not apply to TVLT and that significantly higher rates are achievable.

Beyond practically affording full diversity gain, robust coding gains, and high rates, TVLT also enables convenient performance analysis and design using the EXIT method. Previously, the EXIT chart analysis has been developed for binary and multilevel codes, but it has been limited to SISO systems. It has been shown that in generating the EXIT chart for turbo codes with TVLT, the performance is averaged over channels specified by the singular values of the channel matrix. In particular, for the two transmit antenna case, two eigenvalues are sufficient to specify the region of convergence of the turbo code. It was also shown that this region of convergence can be applied to evaluate the FER of the code. Subsequently, the EXIT chart was found to be a useful tool in the design and analysis of turbo space-time codes.

Finally, various turbo space-time codes with TVLT were demonstrated by simulations and by FER analysis. These codes display all the properties of full diversity, gain and rate as predicted by the analysis and overall have excellent performance with a gap of only 2 dB to outage capacity.

Chapter 4

Multilevel Turbo Space-time Coding

In the last chapter, the method of using TVLT to design full diversity turbo space-time codes is proposed and three codes for two transmit antennas with rate 2, 3, 4 bits/s/Hz, respectively, are presented. In this chapter, the method to design codes with higher data rate without increasing the number of transmit antennas is studied. According to [1], for a b bits/s/Hz space-time code to achieve r order transmit diversity, the trellis complexity (number of states) is at least $2^{b(r-1)}$. That is, the trellis complexity increases exponentially with the required data rate.

To achieve high data rate with practical complexity, multilevel codes (MLC) [31] can be used. With multilevel coding, the data bits are divided into several groups and each group is encoded by an individual encoder. Consequently, for a given total data rate, the data rate required for each individual encoder is lowered. Then the trellis complexity of each individual encoder is controlled. Multilevel space-time coding is first studied in [1], and later in [32] (only for fast fading channels).

To decode MLC, multi-stage decoding (MSD) is proposed in [31]. At the first decoding stage, the first level code is decoded treating signals from higher levels as interference. At the second decoding stage, the contribution of the first level is removed from the channel observation while treating signals from higher level as interference. All the other levels are then decoded in the same fashion, sequentially.

In this chapter, multilevel turbo-STCs with TVLT are proposed. With TVLT, full diversity can be guaranteed. Multidimensional set partition tech-

niques are also used in the proposed scheme. The advantage of multidimensional set partition is to increase the Euclidean distance between the modulation points seen by the codes applied at higher levels. The scheme proposed in this chapter is referred to as *multilevel turbo-STC with TVLT*. For simplicity of representation, in the rest of this chapter the scheme is also referred to as *multilevel turbo-STC* without confusion.

To decode the multilevel turbo-STC, an iterative multi-stage decoding (iterative MSD) algorithm is proposed. In conventional MSD, only the contributions of lower level codes are cancelled. The decision of the higher level code is not used to help the decoding of lower level code. In iterative MSD however, when decoding of a certain level is performed after the first iteration, the soft decisions of all other levels from the previous iteration are used to remove their contributions from the channel observations. Consequently the system performance can be improved. At the same time, since turbo decoder is iterative anyway, the implementation of iterative MSD with turbo-STC will not cause much complexity increase.

As an example of multilevel turbo-STC, a two level, 5 bits/s/Hz code with 16 QAM modulation for two transmit antennas is proposed. Simulation results are also presented and are compared to the outage capacity.

The rest of the chapter is organized as follows. In section 4.1, the encoder structure is described. Section 4.2 presents the decoding algorithm. The simulation results are presented in section 4.3. Section 4.4 draws conclusions.

4.1 Multilevel Turbo-STC Encoder

The structure of the multilevel turbo-STC encoder is shown in Figure4.1. At each time interval t, the information bits are partitioned into W groups of $n_s^1, ..., n_s^W$ bits, respectively, and dispatched to W *individual* turbo-STC encoders to be encoded. In this chapter, the term *individual* encoder/decoder is used to denote the turbo-STC encoder/decoder for each level. This term should be differentiated from the term *component* encoder/decoder of which each individual turbo-STC encoder/decoder is composed. For the multilevel turbo-STC studied in this chapter, each individual turbo-STC encoder/decoder is composed of two component encoders/decoders.

Denote the information/systematic bits input to the w-th individual encoder as $\mathbf{s}^w(t) = \left[s_0^w(t), ..., s_{n_s^w-1}^w(t) \right]$, $w = 1, ..., W$. After encoding, individual encoder $1, ..., W$ generates $n_p^1, ..., n_p^W$ parity bits respectively, denoted as

58

$\mathbf{p}^w(t) = \left[p_0^w(t), ..., p_{n_p^w-1}^w(t) \right]$, $w = 1, ..., W$. Then the rate of each individual encoder is

$$R_w = \frac{n_s^w}{n_s^w + n_p^w}, w = 1, ..., W.$$

Let $Q = \sum_{w=1}^{W} \left(n_s^w + n_p^w \right)$ denote the total number of bits output by all W individual encoders. Then the overall coding rate is

$$R = \frac{\sum_{w=1}^{W} n_s^w}{Q}.$$

Let $\boldsymbol{\nu}^w(t) \triangleq [\mathbf{s}^w(t), \mathbf{p}^w(t)]$ denote the coded bits, including both systematic bits and parity bits, from the w-th individual encoder. Further let $\boldsymbol{\nu}(t) \triangleq \left[\boldsymbol{\nu}^1(t), ..., \boldsymbol{\nu}^W(t) \right]$ denote the coded bits from all individual encoders. The coded bits $\boldsymbol{\nu}(t)$ are mapped into n_T symbols $\mathbf{c}(t) = [c_1(t), ..., c_{n_T}(t)]^T$ through a given mapping $\mathcal{M}$, i.e., $\mathbf{c}(t) = \mathcal{M}(\boldsymbol{\nu}(t))$. In the proposed multilevel turbo-STC scheme, $\mathcal{M}$ is a multidimensional set partition. With TVLT as described in Chapter 3, the vector of symbols $\mathbf{c}(t)$ are multiplied by a unitary matrix $\mathbf{G}(t)$ to obtain another vector $\mathbf{x}(t) = \mathbf{G}(t)\mathbf{c}(t)$, and are transmitted through n_T antennas.

The major design procedure of MLC encoder is to determine the rate of each individual encoder. The rate design of MLC over AWGN channel is studied in [31] [33], while the rate design for MLC over the fast fading MIMO channel is studied in [32]. The basic idea is to treat the MLC system as a group of individual codes transmitting over channels with different capacities. The lowest (first decoded) level has the lowest signal to interference and noise ratio (SINR) since the interference from other levels is not removed. For higher levels, the interference from lower levels has been removed before decoding and the SINR is improved. Hence the capacity of the channel seen by a higher level is larger than that seen by a lower level. The code rates for each levels should then be assigned according to these different channel capacities. For the AWGN and fast fading channels considered in [31], [32], and [33], the channel capacities for each level can be easily computed since the power of interference from other levels can be computed.

For the block (quasi-static) fading MIMO channel model as studied in this report, the channel capacity is changing from one codeword transmission to

another. This means the optimum rates for each layer should also change adaptively according to each channel realization. Adaptive rate transmission can be implemented in a system with feedback channels, which is an interesting future work but is not considered in this report.

In this report, the rate design for each level is performed empirically and takes advantage of the multidimensional set partition (MDSP) [17]. With MDSP, the higher level has a higher SNR than the lower level because of the enlarged Euclidean distance between the modulation points. Hence the MIMO channel (including the modulator) seen by the higher levels have higher capacities than the lower levels. Then the rate of each level should be assigned in an increasing order from the lowest level to the highest. But the exact rate of each level is determined empirically. Encoders of the higher level can also be designed with less trellis complexity while achieving comparable performance to the lower level.

The method of applying MDSP to design multilevel turbo-STC is demonstrated through an example. A rate 5 bits/s/Hz, two level ($L = 2$) turbo-STC, with two transmit antennas ($n_T = 2$) and 16-QAM modulation is considered. The structure of the individual encoders is shown in Figure 3.2 in Chapter 3. The parameters of these two turbo-STC encoders are shown in Table 4.1. At each time interval t, encoder 1 outputs systematic bits $s_0^1(t)$, $s_1^1(t)$, $s_2^1(t)$ and parity bits $p_0^1(t)$, $p_1^1(t)$, while encoder 2 outputs systematic bits $s_0^2(t)$, $s_1^2(t)$, and parity bits $p_0^2(t)$.

The 2-D set partition of 16-QAM is shown in Figure 4.2. After two times partition, each subset $C_0, ..., C_3$ contains only 4 points with doubled minimum Euclidean distance between points. Based on the 2-D set partition of 16-QAM, the 4-D set partition of 2×16 QAM is shown in Figure 4.3. After four times partition, 16 subsets $\Psi_0, ..., \Psi_{15}$ are obtained with 16 points in each subset. It can be shown that the minimum Euclidean distance between the modulation points in each subset is twice as large as that of the original constellation. In the example code, four bits $\{p_0^1(t), p_1^1(t), s_0^1(t), s_1^1(t)\}$ are used to select a subset in $\{\Psi_0, ..., \Psi_{15}\}$, as demonstrated in Figure 4.3. The remaining four bits $\{s_2^1(t), p_1^2(t), s_0^2(t), s_1^2(t)\}$ are used to select a point in the subset. That is, all the bits output by encoder 2 are mapped into a point in one of the subsets $\Psi_0, ..., \Psi_{15}$, which has a twice as large minimum Euclidean distance as the original constellation used by encoder 1. Hence, encoder 2 should be designed to have a higher rate, and/or less trellis complexity than encoder 1. In fact, as shown in Table 4.1, encoder 1 is designed to be rate 3/5 and each component encoder has 16 states. In contrast, encoder 2 is

designed to have rate 2/3 and each component encoder has 8 states.
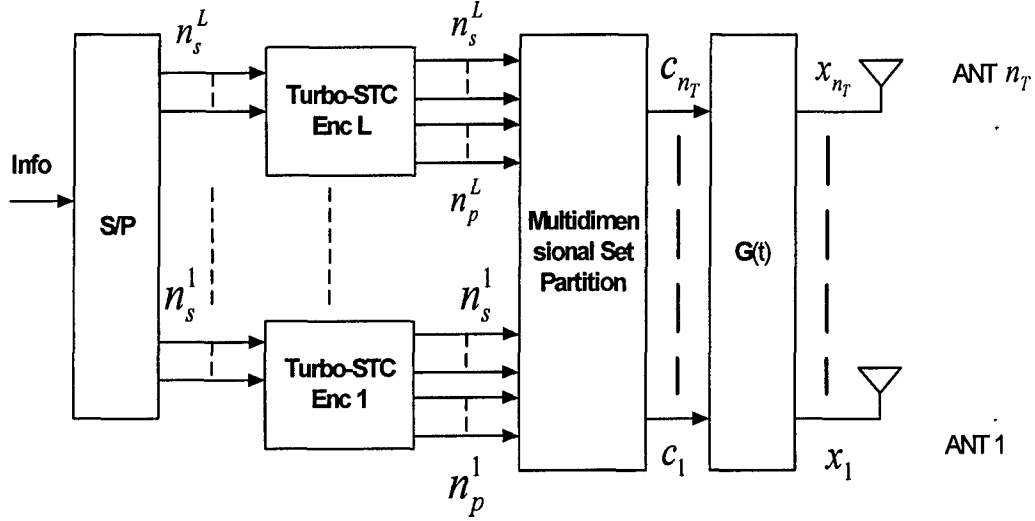
Figure 4.1: Structure of the encoder of multilevel turbo space-time code, with set partition and TVLT.

Table 4.1: Parameters of the Two Turbo-STCs Used to form the Multilevel Turbo-STC

Code	Rate	v	$H^0(D)$	$H^1(D)$	$H^2(D)$	$H^3(D)$	$H^4(D)$	$F(D)$
Enc 1	2/3	3	6_8	1_8	2_8		0	3_8
Enc 2	3/5	4	10	01	02	04	0	1

4.2 Iterative Multistage Turbo-STC Decoder

In this section, the decoding algorithm for multilevel turbo-STC is studied. The channel model used is the same as (3.1) and (3.2) , and is reproduced below for convenience. The received signal at time interval t is

$$\mathbf{r}(t) = \mathbf{H}\mathbf{G}(t)\mathbf{c}(t) + \mathbf{n}(t), \tag{4.1}$$

61

Figure 4.2: Partition of 16 QAM constellation with increasing minimum subset distances.

Figure 4.3: Partition of a 2 × 16 QAM constellation based on the 16 QAM set partition.
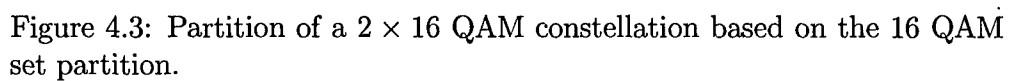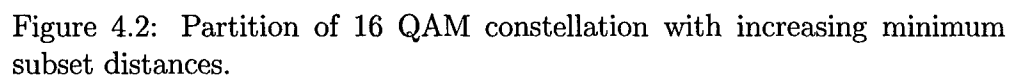
where $\mathbf{c}(t)$ is the $n_T \times 1$ vector of the coded symbols with energy E_s/n_T; $\mathbf{r}(t)$ is the $n_T \times n_R$ received signal vector; $\mathbf{H}$ is the $n_T \times n_R$ channel gain matrix which consists of complex-valued scalars $h_{ij}, i = 1, ..., n_R, j = 1, ..., n_T$, modeled as zero-mean, mutually independent, identically distributed Gaussian random variables with unity variance; $\mathbf{G}(t)$ is the $n_T \times n_T$ random unitary matrix. The noise term $\mathbf{n}(t)$ is modeled by zero-mean, additive white Gaussian noise (AWGN) with variance $N_0/2$ per dimension.

4.2.1 Iterative MSD Decoder

The block diagram of the iterative MSD algorithm is shown in Figure 4.4. Corresponding to W individual encoders, there are W individual turbo decoders at the receiver. Since the coded bits from all individual encoders are mapped together into a set of symbols and transmitted, the channel observation must be first decoupled before being passed to the individual decoders to be decoded. The whole MSD decoder works in an iterative fashion. At each iteration, the w-th signal decoupler computes the decoupled channel observation for the w-th individual decoder, suppressing the contribution of the signals from other levels by using the *a posteriori* probability (APP) of the transmitted vectors of bits computed by their corresponding individual decoders in the last iteration. The algorithm for each individual decoder is the same as in [34] [7] with the additional function of computing the APPs for the vector of coded bits. The rest of this subsection describes the details of the decoupler and decoder in one iteration. For simplicity of representation and to avoid confusion, the iteration index is omitted in the following expressions.

Let $\mathbf{b}_k^m = [b_0, ..., b_{m-1}]$ denote a length m binary vector that represents a nonbinary integer k, i.e., $k = \sum_{i=0}^{m-1} b_i 2^i$. The decoupled channel observation for the vector of bits $\boldsymbol{\nu}^w(t)$ transmitted by the w-th individual encoder can be represented as the sets of log-likelihoods

$$\left\{ \log \left(P \left(\mathbf{r}(t) | \boldsymbol{\nu}^w(t) = \mathbf{b}_k^{n_s^w + n_p^w} \right) \right), k = 0, ..., 2^{n_s^w + n_p^w} - 1 \right\},$$

$t = 1, ..., N$. Let B_k^w denote the set of all possible vectors of $\boldsymbol{\nu}(t)$ such that $\boldsymbol{\nu}^w(t) = \mathbf{b}_k^{n_s^w + n_p^w}$, i.e.,

$$B_k^w = \left\{ \boldsymbol{\nu}(t) \mid \boldsymbol{\nu}^w(t) = \mathbf{b}_k^{n_s^w + n_p^w} \right\}.$$

63
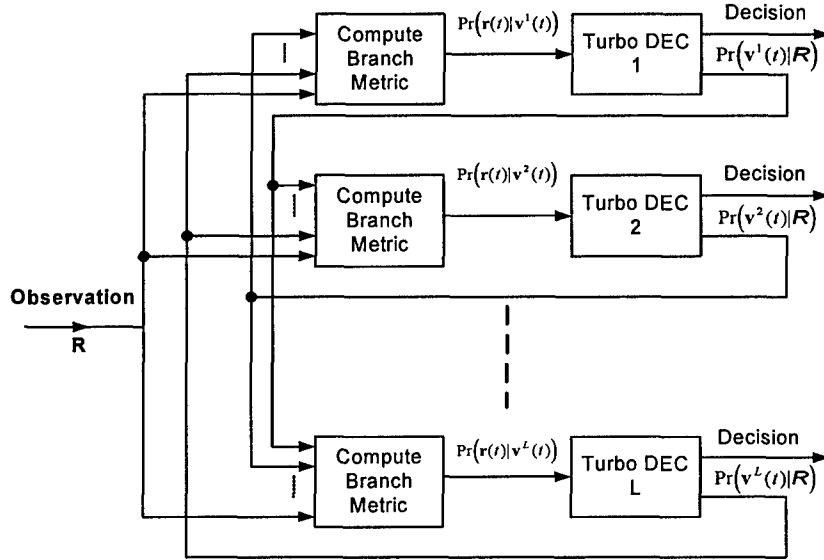
Figure 4.4: Structure of the iterative MSD for multilevel turbo-STC with L levels.

Also define C_k^w as the set of modulated symbol vectors corresponding to the bits vectors in B_k^w, that is,

$$C_k^w \triangleq \{ \mathbf{c}(t) = \mathcal{M}(\boldsymbol{\nu}(t)) \mid \boldsymbol{\nu}(t) \in B_k^w \},$$

Then

$$\log \left(P \left(\mathbf{r}(t) | \boldsymbol{\nu}^w(t) = \mathbf{b}_k^{n_s^w + n_p^w} \right) \right) \tag{4.2}$$

$$= \log \left(\sum_{\boldsymbol{\nu}(t) \in B_k^w} P(\mathbf{r}(t)|\mathbf{c}(t) = \mathcal{M}(\boldsymbol{\nu}(t))) \prod_{\substack{i=1 \\ i \neq w}}^{W} P_A \left(\boldsymbol{\nu}^i(t) = \mathbf{b}_k^{n_s^i + n_p^i} \right) \right)$$

$$= \log \left(\sum_{\mathbf{c}(t) \in C_k^w} \exp \left(-\frac{\|\mathbf{r}(t) - \mathbf{HG}(t)\mathbf{c}(t)\|^2}{N_0} + \sum_{\substack{i=1 \\ i \neq w}}^{W} L_A \left(\boldsymbol{\nu}^i(t) = \mathbf{b}_k^{n_s^i + n_p^i} \right) \right) \right),$$

where

$$L_A \left(\boldsymbol{\nu}^i(t) = \mathbf{b}_k^{n_s^i + n_p^i} \right) \triangleq \log \left(P_A \left(\boldsymbol{\nu}^i(t) = \mathbf{b}_k^{n_s^i + n_p^i} \right) \right),$$

64

$k = 1, ..., 2^{n_s^i + n_p^i} - 1, i = 1, ..., W$ is the *a priori* about the bit vector transmitted from the i-th individual encoder. In the proposed iterative MSD scheme, the *a priori* $L_A \left(\boldsymbol{\nu}^i(t) = \mathbf{b}_k^{n_s^i + n_p^i} \right)$, $i = 1, ..., W$, used in the current iteration is set to be equal to the APP generated in the last iteration. Let

$$L_P \left(\boldsymbol{\nu}^i(t) = \mathbf{b}_k^{n_s^i + n_p^i} \mid \mathbf{R} \right) \triangleq \log \left(P \left(\boldsymbol{\nu}^i(t) = \mathbf{b}_k^{n_s^i + n_p^i} \right) \mid \mathbf{R} \right) \right)$$

be the APP calculated by the W individual decoders from the last iteration, where the matrix $\mathbf{R} \triangleq [\mathbf{r}(1), ..., \mathbf{r}(N)]$ denotes the channel observations of the whole codeword. Then,

$$L_A \left(\boldsymbol{\nu}^i(t) = \mathbf{b}_k^{n_s^i + n_p^i} \right) = L_P \left(\boldsymbol{\nu}^i(t) = \mathbf{b}_k^{n_s^i + n_p^i} \mid \mathbf{R} \right).$$

In the first iteration, $L_A \left(\boldsymbol{\nu}^i(t) = \mathbf{b}_k^{n_s^i + n_p^i} \right)$ is set to be zero. The method used to compute the APP of the vector of coded bits $\boldsymbol{\nu}^i(t)$ is a straightforward extension of the computation of the systematic bits $\mathbf{s}^i(t)$ [35].

4.2.2 List Sphere Decoder

The purpose of multilevel codes is to avoid the exponentially increase in trellis complexity and consequently the decoder complexity when the data rate increases. This goal has been achieved by the encoder and decoder algorithm presented in the last two subsections. However, the complexity of the decoupler, which computes decoupled channel observation for each level, still increases exponentially with the number of transmitted bits at each time interval, as shown in (4.2). In (4.2), for the w-th level, the set C_k^w includes all possible transmitted symbol vectors $\mathbf{c}(t)$, in which the bits from the w-th level is a specific combination $\mathbf{b}_k^{n_s^i + n_p^i}$. Then C_k^w has 2^{q_w} elements, where

$$q_w = \sum_{\substack{i=1 \\ i \neq w}}^{W} \left(n_s^i + n_p^i \right).$$

That is, 2^{q_w} times $\exp(\bullet)$ function calculation is needed to carry out (4.2).

To lower the complexity of the decoupler, the list sphere decoder (LSD) [36] can be used. The function of the LSD is briefly introduced here while the details are in [36]. Let C denote the set of all possible $n_T \times 1$ symbol

vectors. Given the channel model (4.1), let $\widehat{\mathbf{c}}(t)$ be an unconstrained ML estimate of $\mathbf{c}(t)$, i.e.,

$$\widehat{\mathbf{c}}(t) = \left(\mathbf{G}(t)^{\dagger}\mathbf{H}^{\dagger}\mathbf{H}\mathbf{G}(t)\right)^{-1}\mathbf{H}\mathbf{G}(t)\mathbf{r}(t),$$

the list sphere decoder search for the set $C_{LSD}(t)$

$$C_{LSD}(t) \triangleq \left\{\mathbf{c}(t) \mid \mathbf{c}(t) \in \arg \min_{\mathbf{c}(t)\in C}^{N_{cand}} \left\{\|\mathbf{c}(t) - \widehat{\mathbf{c}}(t)\|^2\right\}, \|\mathbf{c}(t) - \widehat{\mathbf{c}}(t)\|^2 \leq \delta^2\right\}$$

where $\arg \min_{\mathbf{c}(t)\in C}^{N_{cand}} \{\|\mathbf{c}(t) - \widehat{\mathbf{c}}(t)\|^2\}$ denotes the set that includes N_{cand} nearest symbol vectors to $\widehat{\mathbf{c}}(t)$; δ is the search radius. The denotation N_{cand} is borrowed from [36], where it means number of candidates. So, all the symbol vectors included in the set $C_{LSD}(t)$ are within distance range δ^2 from $\widehat{\mathbf{c}}(t)$; and there are at most N_{cand} vectors in $C_{LSD}(t)$. Usually N_{cand} is set to be much less than 2^Q, the number of all possible transmitted symbol vectors. After $C_{LSD}(t)$ is found, the set C_k^w in the third line of (4.2) is replaced with $C_{k,LSD}^w(t)$, the intersection of C_k^w and $C_{LSD}(t)$. That is,

$$C_{k,LSD}^w(t) \triangleq C_k^w \cap C_{LSD}(t).$$

If $C_{k,LSD}^w(t) = \varnothing$, the decoupled channel observation, or the log-likelihood in (4.2) is set to be a default limit value. Since there are fewer elements in $C_{LSD}(t)$ than in C_k^w, the complexity of computing (4.2) is significantly lowered.

The two parameters N_{cand} and δ controls the complexity and performance of the signal decoupler. If N_{cand} and δ are set to be too small, few symbol vectors will be included in $C_{LSD}(t)$ to be used in computing (4.2), and the decoupled channel observation might be very inaccurate. Thus the performance of the receiver could be significantly degraded. Of course if N_{cand} and δ are set to be too large then the complexity reduction will not be satisfactory. Usually the values of N_{cand} and δ are selected empirically.

4.3 Simulation Results

In this subsection the simulation results for the two-level, 5 bits/s/Hz, 16 QAM modulation (before TVLT) turbo STC for two transmit antennas are

presented. The details of this code have been presented in section 4.1. The length of the interleaver used in each individual turbo space-time encoder is $N = 1024$. Two receive antennas are used at the receiver. The channel is block Rayleigh fading as described in (4.1). The performance measured is FER against SNR (dB).

Both full complexity iterative MSD decoder and reduced complexity decoder with LSD are simulated. For the LSD used in the simulation, N_{cand} is set to be 40. In contrast, the number of all possible 2×16 QAM symbol vectors is 256. That is, the complexity of the signal decoupler is reduced to about $1/6$ of that of the decoupler without LSD. The search radius δ is set to be $\sqrt{382/\text{SNR}}$ empirically, such that δ decreases with SNR. For example, for SNR=18 dB, $\delta \approx 2.5$.

The simulation results are provided in Figure 4.5 for the proposed multilevel turbo-STC using full complexity iterative MSD decoder and reduced complexity decoder with LSD, respectively. The outage probability curve is also provided for reference. From the figure it is observed that using the full complexity iterative MSD decoder, full space diversity is achieved since the FER curve is parallel to the outage probability curve. And the performance is only 2 dB away from the outage probability.

It is also observed that the FER curve for the reduced complexity decoder with LSD diverges from that of the full diversity decoder, showing that full diversity is not achieved at higher SNR. However, at FER=0.01, the performance degradation is only 1.5 dB compared to the full complexity decoder, which may still be considered a satisfactory trade off between performance and complexity.

4.4 Chapter Summary

In this chapter, the multilevel turbo STC scheme is proposed to avoid the exponentially increasing decoding complexity. An iterative MSD decoding algorithm is also proposed. Full diversity and close to capacity performance is demonstrated by simulations. A reduced complexity decoder with LSD is also proposed to provide trade off between the complexity and performance.
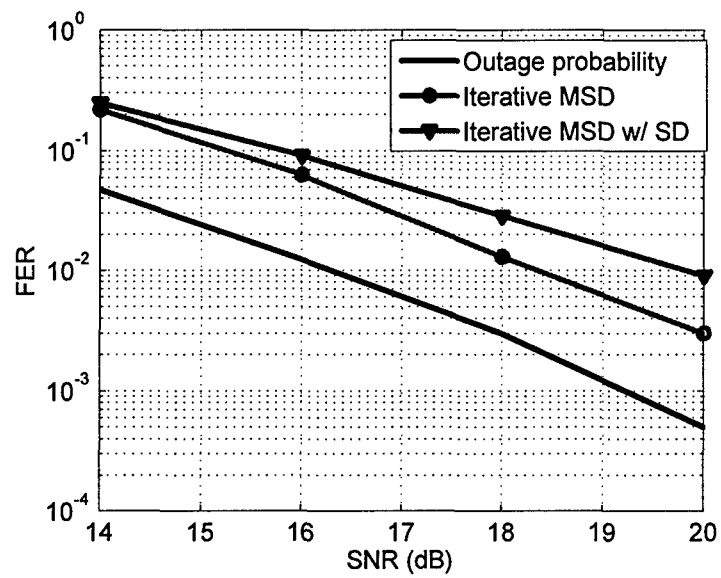
Figure 4.5: FER performances of the two level turbo space-time codes over 2×2 block Rayleigh fading channel.

Chapter 5

Layered Turbo Space-time Coding

In Chapter 3, the turbo-STC with TVLT scheme is studied mostly for two transmit antenna and low to moderate data rate cases. The reason is that with that scheme the decoding complexity increase exponentially with the number of antennas and/or data rate. Multilevel turbo-STC is proposed in Chapter 4 to design codes with a higher data rate without exponentially increasing decoding complexity. But when very high data rate is required and a large number of transmit antennas is used, the complexity of multilevel turbo-STC is still very high. In this chapter layered turbo space-time coding (LTST) is presented to design low complexity MIMO systems with a large number of transmit and receive antennas.

Layered MIMO systems avoid the high decoding complexity by avoiding joint decoding of the signal from all transmit antennas. In these systems the signals from each transmit antenna or each antenna group, referred to as layers, are first separated and then the separated signals are decoded. To separate the signals belonging to a given layer from other layers, the signals from other layers are treated as interference and suppressed with either linear or nonlinear interference suppression techniques. Various layered MIMO systems have been proposed recently [5] [37] [38] [39] [40] [41].

The layered MIMO systems can be divided into two categories: Bell Lab Architecture of Space-Time (BLAST) and its variants [37] [38] [39] [40] [41], etc., and layered space-time coding (LSTC) [5], etc. The major difference between these two categories is the antennas included in each layer. In BLAST systems each layer contains only one antenna, and traditional, well developed

1-D codes can be used. The major advantage of BLAST systems is simple design. In LSTC, each layer contains multiple (usually two) antennas where space-time coding is applied. Compared to BLAST systems, LSTC has fewer layers to separate at the receiver and for each layer there is one less interferer. With joint decoding the signals from all the antennas within a layer, more transmit diversity is also achieved.

LTST is a special type of LSTC, with turbo-STC applied to each layer. Two LTST structures are proposed and studied in this chapter. One is vertical LTST (V-LTST), the other one is horizontal LTST (H-LTST). The terms *vertical* and *horizontal* are adopted from [42] to indicate how the coding is applied to the layered structure.

In V-LTST, only one turbo-STC encoder is used at the transmitter. The output of the encoder is divided into substreams and transmitted from different layers. At the receiver, the layers are separated using low complexity parallel interference cancellation (PIC) techniques. V-LTST is proposed for MIMO systems with low order modulation such as BPSK and 4-PSK. It is also suitable for low delay communication systems. In H-LTST, an independent turbo-STC encoder with TVLT is used in each layer and successive interference cancellation (SIC) is used at the receiver. The TVLT technique is used to enable ordered SIC (OSIC). H-LTST is used for systems utilizing higher order modulation such as 8-PSK, 16-QAM, etc. The details of these two schemes are presented in the rest of this chapter, after which the advantages and disadvantages of two structures will be made clear.

The rest of this chapter is organized as follows. In Section 5.1 the V-LTST scheme is presented. The H-LTST scheme is presented in section 5.2. Section 5.3 draws conclusions.

# 5.1 Vertical Layered Turbo Space-time Coding

5.1.1 System Model

Consider a MIMO communication system with n_T transmit and n_R receive antennas $(n_T \times n_R)$ operating over a flat, Rayleigh block fading channel. The output of this MIMO channel is represented by $n_T \times 1$ vectors $\mathbf{r}(t) \in C^{n_R}$ that can be expressed

$$\mathbf{r}(t) = \mathbf{H}\mathbf{c}(t) + \boldsymbol{\eta}(t), \tag{5.1}$$

where $\mathbf{c}(t)$ is $n_T \times 1$ vector of transmitted symbols whose energy is E_s/n_T, and the $n_R \times n_T$ matrix $\mathbf{H}$ consists of the channel coefficients. The (i,j) element of $\mathbf{H}$ represents the path gain from transmit antenna j to receive antenna i. The matrix $\mathbf{H}$ consists of complex-valued scalars h_{ij} modeled as zero-mean, mutually independent, identically distributed Gaussian random variables with unit variance. The $n_T \times 1$ vector $\mathbf{c}_t$ contains the symbols transmitted at time t. The noise term $\boldsymbol{\eta}(t)$ is modeled by zero-mean, additive white Gaussian noise (AWGN) with variance $N_0/2$ per dimension.

The proposed V-LTST structure is shown in Figure 5.1 with the top part showing the transmitter. The information data is encoded by a symbol-wise, parallel concatenated space-time turbo encoder, which will be discussed in more detail later in section 5.1.3. Briefly, this is a systematic turbo encoder, which generates a codeword matrix that consists of two rows, with each row transmitted through an antenna. One row of the codeword matrix contains systematic symbols, while the other carries the corresponding parity symbols. With this arrangement, the signals received from the two transmit antenna are treated as a single entity and do not need to be separated. The codeword is interleaved *pair-wise* so that columns of the codeword matrix are preserved. This ensures that the codeword symbols associated with each trellis branch (in this scheme one systematic symbol and its corresponding parity symbol) are transmitted in the same time slot. The function of the interleaver is to decorrelate adjacent codeword symbols and avoid possible burst errors after interference cancellation at the receiver. Following interleaving, the two-row codeword is separated into several substreams, which are modulated and transmitted from groups of two antennas. The substream of the signals transmitted from each antenna group is referred to as a *layer*.

The LTST receiver is shown in Figure 5.1-b. First, the signals received

71
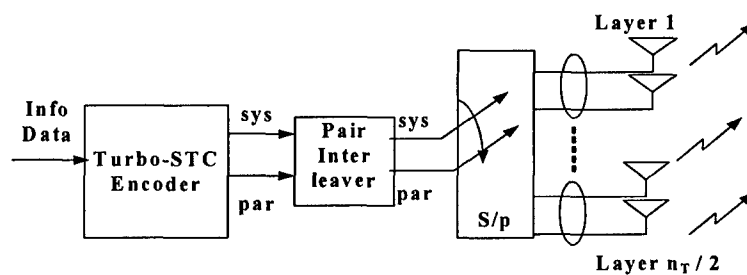
a. V-LTST transmitter
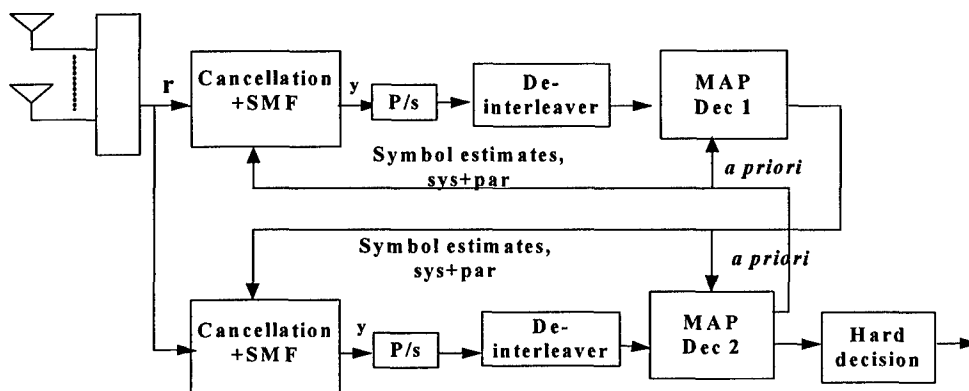
b. V-LTST receiver

Figure 5.1: Structure of the V-LTST transceiver with a single turbo-STC encoder and two antennas per layer.

from different layers are separated by cancelling the estimated signals from other layers (regarded as interference). Then, the separated signals of each layer are re-assembled, de-interleaved to the original order, and passed to the maximum *a posteriori* (MAP) decoders. Soft decisions computed by the decoders are fed back to improve interference cancellation, and the two decoders exchange extrinsic information as in an ordinary turbo decoder. This process repeats for several iterations. The algorithm used at the receiver will be described and analyzed in the next section. The data rate of the proposed scheme is $rn_T \log_2 q$ bits/s/Hz, where q is the cardinality of the symbol constellation and r is the rate of the turbo encoder.

5.1.2 Encoder Design
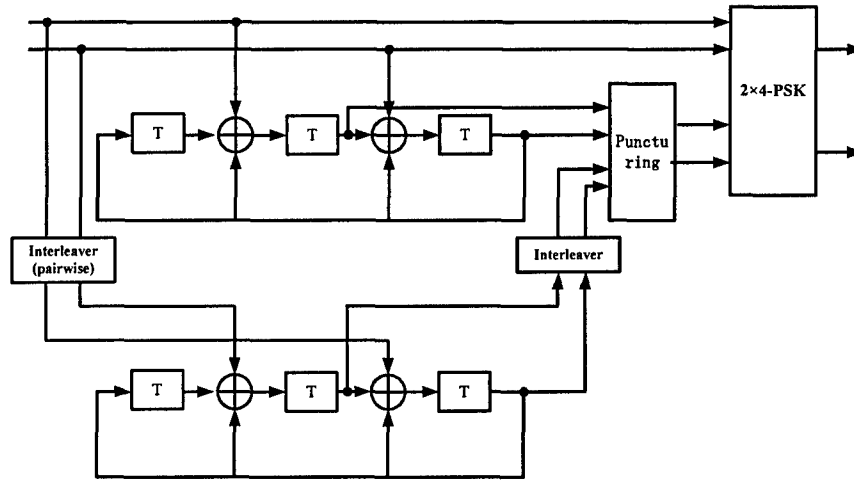
Figure 5.2: Structure of the LTST encoder with 2×4PSK set partition to optimize the Euclidean distance.

In this subsection the design considerations of the V-LTST encoder is discussed. It was proved in [43] that the design criterion for space-time codes which work at low SNR ($\leq$ 10 dB) is to maximize the minimum Euclidean distance between codewords: the same design criterion as the one for traditional trellis coded modulation (TCM). This design criterion motivates the

73

application of the multidimensional set partition techniques [17] [29], originally applied in TCM to increase the minimum Euclidean distance, to the design of the turbo-STC encoder in V-LTST. In particular, the set partition for multidimensional phase modulation proposed in [29] is applied in V-LTST. The multidimensional set partition guarantees that the distance between branches departing and entering the same state in the trellis is at least twice as large as the minimum distance between modulation points. The encoder structure is shown in Figure 5.2. The component convolutional encoder is hand-picked and not guaranteed to be optimal.

5.1.3 Decoder

The turbo decoder used in V-LTST is similar to the log-MAP decoder for turbo-STC [34]. It is necessary to compute *a posteriori probabilities* (APP's) for both the systematic and parity symbols of a codeword. Given the observations for the entire codeword, the log-MAP decoder outputs a set of APP's for each codeword symbol $c_{t,i}$, $i = 1, ..., n_T$, $t = 1, ..., N$, where N is the codeword length or *frame* length. Denote the APP's for $c_{t,i}$ as $P_j = P(c_{t,i} = s_j |$ observations), $j = 1, ..., q$, where $\{s_j, j = 1, ..., q\}$ is the modulation constellation set. The expected value of symbol $\widetilde{c}_{t,i}$

$$\widetilde{c}_{t,i} = \sum_{j=1}^{q} s_j P_j \qquad (5.2)$$

is used in the co-antenna interference cancellation process as explained below. In the first iteration, when no estimate from the decoder is available, $\{\widetilde{c}_{t,i}, t = 1, ..., N, i = 1, ..., n_T\}$ are set to zero.

5.1.4 Interference Cancellation

In V-LTST, the signals from different layers are separated by cancelling estimated signals from other layers. Essentially, the $n_T \mathrm{T} n_R \mathrm{R}$ channel was broken up into $n_T/2$ parallel $2\mathrm{T} n_R \mathrm{R}$ sub-channels. Suppose the desired signal is supplied by the layer with index i. For simple notation, the time index t is dropped. Also, in the following discussion, subscript $\bar{i}$ is used to denote signals associated with all layers *other* than i. Then (5.1) can be rewritten as

$$\mathbf{r} = \mathbf{H}_i \mathbf{c}_i + \mathbf{H}_{\bar{i}} \mathbf{c}_{\bar{i}} + \boldsymbol{\eta}, \tag{5.3}$$

where $\mathbf{H}_i$ is the channel matrix for layer i, an $n_R \times 2$ matrix composed of the two columns of $\mathbf{H}$ pertaining to layer i, and $\mathbf{H}_{\bar{i}}$ is the $n_R \times (n_T - 2)$ matrix that is made up of the rest of the columns of $\mathbf{H}$; $\mathbf{c}_i$ is the 2×1 vector of symbols of layer i, and $\mathbf{c}_{\bar{i}}$ is the $(n_T - 2) \times 1$ vector of symbols from other layers. Denote $\widetilde{\mathbf{c}}_{\bar{i}}$ an estimate of $\mathbf{c}_{\bar{i}}$ computed using (5.2). Interference cancellation is achieved by subtracting, from the received vector $\mathbf{r}$, the estimated contribution of the interference $\mathbf{H}_{\bar{i}} \widetilde{\mathbf{c}}_{\bar{i}}$

$$
\begin{aligned}
\mathbf{y}_i &= \mathbf{r} - \mathbf{H}_{\bar{i}} \widetilde{\mathbf{c}}_{\bar{i}} \\
&= \mathbf{H}_i \mathbf{c}_i + \mathbf{H}_{\bar{i}} (\mathbf{c}_{\bar{i}} - \widetilde{\mathbf{c}}_{\bar{i}}) + \boldsymbol{\eta} \\
&= \mathbf{H}_i \mathbf{c}_i + \mathbf{H}_{\bar{i}} \mathbf{e}_{\bar{i}} + \boldsymbol{\eta},
\end{aligned} \tag{5.4}
$$

where $\mathbf{y}_i$ is the signal from layer i cleaned of interference, and $\mathbf{e}_{\bar{i}} \triangleq (\mathbf{c}_{\bar{i}} - \widetilde{\mathbf{c}}_{\bar{i}})$ is decision feedback error. From (5.4), it can be seen that each layer is a $2 \times n_R$ MIMO channel with interference. Let

$$
\begin{aligned}
\mathbf{R}_i &\triangleq E[(\mathbf{H}_{\bar{i}} \mathbf{e}_{\bar{i}} + \boldsymbol{\eta})(\mathbf{H}_{\bar{i}} \mathbf{e}_{\bar{i}} + \boldsymbol{\eta})^{\dagger}] \\
&= \rho E_s \mathbf{H}_{\bar{i}} \mathbf{H}_{\bar{i}}^{\dagger} + N_0 \mathbf{I},
\end{aligned} \tag{5.5}
$$

be the correlation matrix of the residual interference plus noise, where the superscript denotes complex conjugate transpose. The relative strength of the interference term is given by the normalized mean square error of the decisions feedback $\rho \triangleq E(|e_{\bar{i},l}|^2)/E_s$, where $e_{\bar{i},l}$, $l = 1, ..., n_T - 2$, is an element of the vector $\mathbf{e}_{\bar{i}}$. Then the optimum branch metric used in the decoder is

$$\gamma(\mathbf{y}_i, \mathbf{x}_i) = (\mathbf{y}_i - \mathbf{H}_i \mathbf{x}_i)^{\dagger} \mathbf{R}_i^{-1} (\mathbf{y}_i - \mathbf{H}_i \mathbf{x}_i), \tag{5.6}$$

where $\mathbf{x}_i$ are the symbols to be tested.

The disadvantage of using (5.6) as a branch metric lies wherein the high complexity of inverting the matrix $\mathbf{R}_i$, whose dimensions are $n_R \times n_R$. V-LTST takes a much simpler approach of spatial matched filtering (SMF). Simulation results in section IV demonstrate that in spite of the suboptimal spatial interference suppression, V-LTST achieves performance close to capacity. Following SMF, the desired signal for layer i is:

$$
\begin{aligned}
\widetilde{\mathbf{y}}_i &= \mathbf{H}_i^{\dagger} \mathbf{y}_i \\
&= \mathbf{H}_i^{\dagger} \mathbf{H}_i \mathbf{c}_i + \mathbf{H}_i^{\dagger} \mathbf{H}_{\bar{i}} \mathbf{e}_{\bar{i}} + \mathbf{H}_i^{\dagger} \boldsymbol{\eta} \\
&= \mathbf{A}_i \mathbf{c}_i + \mathbf{B}_i \mathbf{e}_{\bar{i}} + \mathbf{H}_i^{\dagger} \boldsymbol{\eta} \\
&= \mathbf{A}_i \mathbf{c}_i + \mathbf{v}_i + \mathbf{z}_i,
\end{aligned} \tag{5.7}
$$

75

where $\mathbf{A}_i \triangleq \mathbf{H}_i^\dagger \mathbf{H}_i$ is a 2×2 matrix; $\mathbf{B}_i \triangleq \mathbf{H}_i^\dagger \mathbf{H}_{\bar{i}}$ is a $2 \times (n_T - 2)$ matrix; $\mathbf{v}_i \triangleq \mathbf{B}_i \mathbf{e}_{\bar{i}}$ and $\mathbf{z}_i \triangleq \mathbf{H}_i^\dagger \boldsymbol{\eta}$ are respectively, 2×1 vectors of the residual interference and noise term post SMF. It is noted that (5.7) is now an equivalent 2T2R channel model.

Assuming residual interference plus noise, $\mathbf{v}_i + \mathbf{z}_i$, to be AWGN, the following sub-optimum branch metric is used in V-LTST

$$\gamma(\mathbf{y}_i, \mathbf{x}_i) = (N_0')^{-1} (\mathbf{y}_i - \mathbf{H}_i \mathbf{x}_i)^\dagger \mathbf{H}_i \mathbf{H}_i^\dagger (\mathbf{y}_i - \mathbf{H}_i \mathbf{x}_i), \qquad (5.8)$$

where N_0' is the variance of the elements of the vector $\mathbf{v}_i + \mathbf{z}_i$. The variance of interference plus noise N_0' is needed in (5.8) for incorporation of the *a priori* information in the MAP decoding, and is computed as

$$\begin{aligned} N_0' &= E[(\mathbf{v}_i + \mathbf{z}_i)(\mathbf{v}_i + \mathbf{z}_i)^\dagger] && (5.9) \\ &= \frac{1}{2}\left(\rho \frac{E_s}{n_T} \cdot \mathrm{tr}(\mathbf{B}_i \mathbf{B}_i^\dagger) + N_0 \cdot \mathrm{tr}(\mathbf{A}_i)\right), \end{aligned}$$

where $\mathrm{tr}(\cdot)$ is the trace operation. And the signal to interference noise ratio (SINR) after SMF is

$$\begin{aligned} \mathrm{SINR}_i &= \frac{E_s}{n_T N_0'} \\ &= \frac{1}{2\left(\rho\,\mathrm{tr}(\mathbf{B}_i \mathbf{B}_i^\dagger) + \frac{n_T N_0}{E_s}\,\mathrm{tr}(\mathbf{A}_i)\right)} \end{aligned}$$

In the first iteration no soft decision is available to cancel the signals from other layers and $\rho = 1$. The initial SINR_i with $\rho = 1$ will be at most $1/\left(2\mathrm{tr}(\mathbf{B}_i \mathbf{B}_i^\dagger)\right)$, which will not decrease with the $\mathrm{SNR} \triangleq E_s/N_0$. If the data rate is high and the modulation size is large, this initial SINR_i can be too small for the decoder to generate good enough soft decisions, to be usable for cancellation in the next iteration. In this report it is found that V-LTST is only suitable for small size modulation such as 4-PSK and BPSK.

5.1.5 Space Interleaving

In V-LTST, The dominant error events for layered systems are caused by the channel gain matrix for one layer being nearly "parallel" (opposite to orthogonal) to that of other layer(s). When the channel gain matrix of one layer

is almost "parallel" to that of the other layer(s), the interference between layers will be strong. Consider the SMF used in (5.7). When the channel gain matrix of $\mathbf{H}_i$ for layer i is orthogonal to $\mathbf{H}_{\bar{i}}$, or $||\mathbf{H}_i^\dagger \mathbf{H}_{\bar{i}}||^2 = 0$, there will be no interference from other layers at all. The notation $|| \cdot ||^2$ represents the Frobenius norm. Conversely, if for some channel realizations $||\mathbf{H}_i^\dagger \mathbf{H}_{\bar{i}}||^2$ is large, the interference from other layers will be strong. To improve the system performance in these cases, the combination of antennas in each layer during the transmission can be alternatively changed, which is referred to as space interleaving. A 4T4R system will be used as an example. Let $\mathbf{H} = [\mathbf{h}_1\ \mathbf{h}_2\ \mathbf{h}_3\ \mathbf{h}_4]$ where $\mathbf{h}_i,\ i = 1, ..., 4$ are columns of $\mathbf{H}$. The combination of antennas in each layer, as it evolves with time, is illustrated in Table 5.1. As a result of space interleaving, if at some time interval $||\mathbf{H}_i^\dagger \mathbf{H}_{\bar{i}}||^2$ is large, it is possible that at another time interval with another combination, $||\mathbf{H}_i^\dagger \mathbf{H}_{\bar{i}}||^2$ is small.

Table 5.1: An Example of Space Interleaving of the Transmit Antennas in Two Layers

time	layer 1	layer 2	H_1	H_2
1	ant 1,2	ant 3,4	h_1h_2	h_3h_4
2	1,3	2,4	h_1h_3	h_2h_4
3	1,4	2,3	h_1h_4	h_2h_3
4	1,2	3,4	h_1h_2	h_3h_4
...	...	...	...	...

Similar techniques are proposed for single antenna per layer systems such as [37] [39] for different purposes. In those schemes, a signal from each layer is cycling through all the transmit antennas. In this fashion, each layer will achieve more diversity.

5.1.6 Complexity Analysis

In this subsection and next subsection the V-LTST scheme is going to be compared to existing schemes with the same number of antennas, data rate, and comparable performance. The turbo-greedy algorithm [41] is a turbo coded vertical-BLAST (V-BLAST) systems, with simplified joint maximum

likelihood (ML) demodulation, referred to as turbo-greedy algorithm, of the bits transmitted from all transmit antennas. The threaded space-time (TST) scheme [40] uses a transmitter structure similar to diagonal BLAST (D-BLAST), with a minimum mean square error (MMSE) demodulator to separate the signals from each transmit antennas.

Now the complexity of V-LTST with that of other MIMO schemes with similar performance is compared. The complexity of interference subtraction and SMF is only $O(n_T)$. Typically, the complexity of the V-LTST receiver is dominated by the turbo decoder whose log-MAP decoding has a complexity of $O(\nu 2^{\log q})$, where ν is the number of states of the convolutional encoder and q is the modulation size. In contrast, the complexity of ML spatial demodulation is $O(\exp(n_T))$ and that of its simplified version, the turbo-greedy algorithm, is less than $O(\exp(n_T))$, but higher than $O(n_T^4)$ [41]. As another point of comparison, the complexity of the threaded space-time (TST) scheme [40] with MMSE interference suppression is $O(n_T^4)$. Thus for $n_T = 4$, $q = 4$, $\nu = 8$, the complexity of V-LTST is $O(32)$ compared to $O(256)$ for turbo-greedy and MMSE interference suppression.

5.1.7 Numerical Results

Numerical results for the V-LTST scheme are presented for 4×4 and for 8×8 configurations. For 4-PSK modulation, the data rate for the 4×4 system is 4 bits/s/Hz, and for the 8×8 system it is 8 bits/s/Hz. Both systems are full rate. The channel is assumed to be constant over blocks of 130 channel uses. Consequently, the frame length for 4×4 system is 260 symbols (130 channel uses $\times$ 2 layers), and for the 8×8 system is 520 symbols. The SNR is defined E_s/N_0, i.e., the ratio of the total transmitted power to the noise power.

To determine the number of iterations, a simple stop criterion is used in V-LTST, where the iterations stop whenever two successive iterations yield the same hard decision. For all the V-LTST simulation results presented below, the average number of iterations varied from 3 to 5. Numerical results shown for TST and turbo-greedy algorithms are lifted from [40] and [41], respectively.

Figure 5.3 shows the frame error rate (FER) for 4×4 systems. It can be observed that V-LTST, TST, and turbo-greedy curves are approximately parallel indicating the same space-diversity gain. V-LTST outperforms turbo-greedy coding by 0.5 dB and outperforms TST by approximately 1.3 dB.
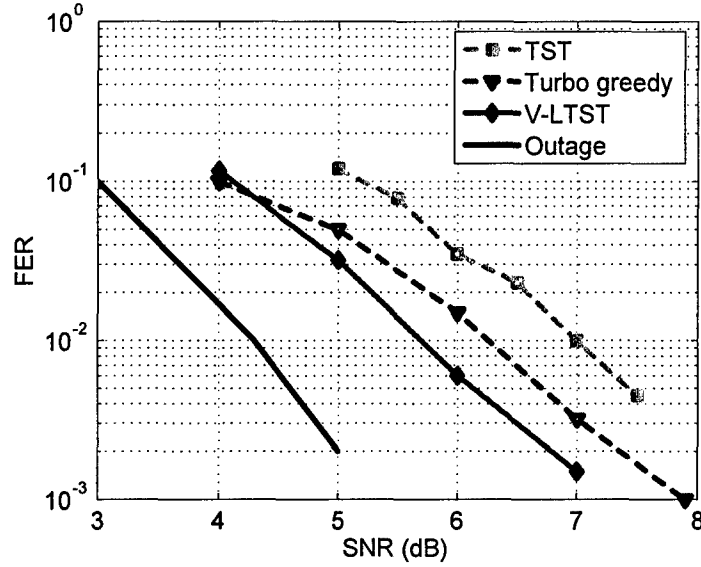
Figure 5.3: FER comparison of V-LTST and other schemes, 4×4, 4 b/s/Hz.

It can also be observed that the performances of both V-LTST and turbo-greedy are within 2 dB range of the outage probability. Figure 5.4 shows the FER comparison for 8×8 systems. It can be observed that V-LTST and turbo-greedy coding have similar performances and outperform TST by about 1 dB.

5.2   Horizontal Layered Turbo Space-time Coding

V-LTST achieves close to outage probability performance with simple, low complexity interference subtraction to separate the signals from different layers. But V-LTST is only suitable for low order modulation systems. In this section, H-LTST is then proposed for systems that require a higher rate and higher order modulations.
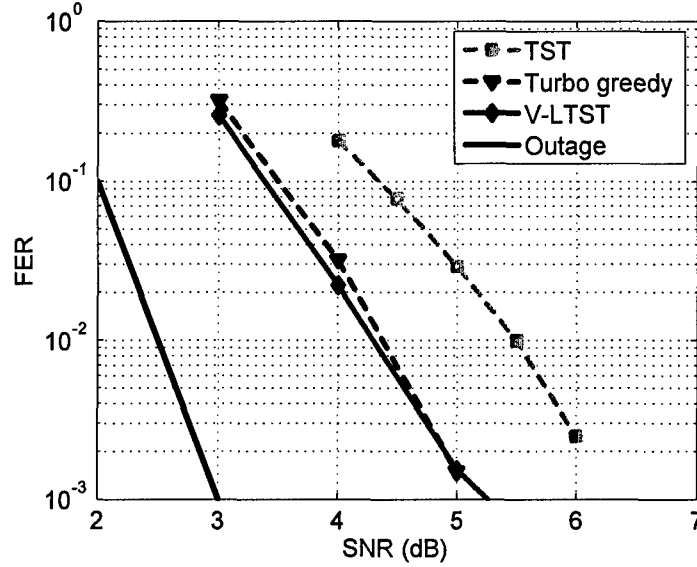
Figure 5.4: FER comparison of V-LTST and other schemes, 8×8, 8b/s/Hz.

5.2.1 System Model

The structures of the H-LTST transmitter and receiver are shown in Figure 5.5. At the transmitter, the n_T transmit antennas are partitioned into $n_T/2$ layers with two antennas in each layer. An independent turbo-STC encoder is used in each layer. The $n_T/2$ encoders may be different. In this chapter however, only the case where the encoders for every layer are the same is considered. The TVLT technique is also applied to each layer. That is, the coded symbols are multiplied by a random unitary matrix before being transmitted.

At the H-LTST receiver SIC is used to separate the layers. That is, the interference from the previously detected/decoded layers are cancelled while the interference from other undetected layers are nulled by ZF filtering. After the cancel-null operation, the signals for the desired layer is obtained and decoded.

For SIC detector, the detection order is important since the layer with the least decoding error probability should be detected first [38], to minimize the effect of error propagation and then to minimize the overall error rate of the
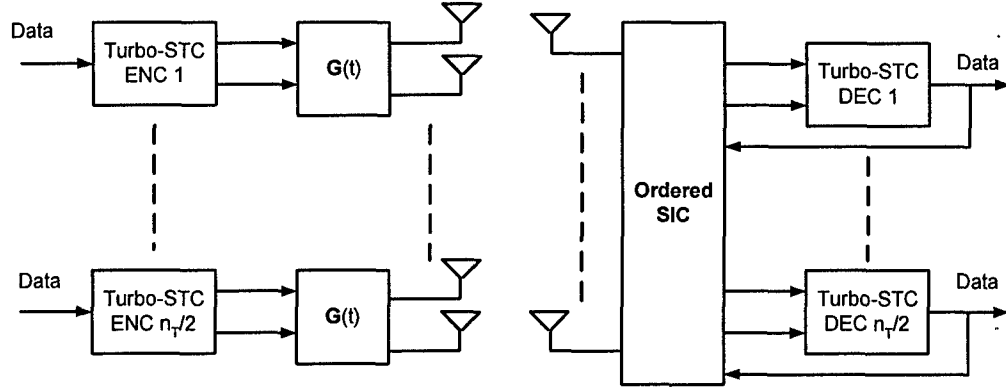
Figure 5.5: Structure of H-LTST with independent turbo-STC encoder/decoder for each layer.

whole system. In H-LTST, TVLT is applied to each layer. Hence whether or not the decoder of a certain layer will converge to the correct decision (error free) can be predicted with high accuracy, using the method presented in Chapter 3. Then the layer that is predicted to converge should be detected first and the optimum detection order can be determined.

In the previous proposed layered space-time coding (LSTC) scheme [5], however, ordered SIC, or OSIC, is not applicable and the layers are detected in an arbitrary but fixed order independent of the current channel condition. To mitigate the performance loss due to lack of optimum detection order, non-constant power transmission is used. In [5], to take advantage of the fact that later detected layers have a higher diversity order, the earlier detected layers are assigned a higher transmit power than the later layers. This non-constant power transmission, however, leads to an increased requirement for the amplifier dynamic range and then the amplifier cost.

5.2.2 Ordered SIC

The channel model is the same as in (5.1) and (5.3), except that the transmitted signal of each layer is multiplied by the random unitary matrix $\mathbf{G}(t)$, referred to as TVLT in Chapter 3. Let $\mathbf{c}(t)$ be the $n_T \times 1$ vector of coded symbols to be transmitted at time interval t, each having energy E_s/n_T. Also let $\mathbf{c}_k(t)$ be the 2×1 vector of coded symbols from the k-th layer.

81

That is $\mathbf{c}(t) = \left[\mathbf{c}_1^T, ..., \mathbf{c}_{n_T/2}^T \right]^T$, where $(\cdot)^T$ denotes matrix transpose. Let $\mathbf{x}_k(t) = \mathbf{G}(t)\mathbf{c}_k(t)$ be signal after TVLT and $\mathbf{x} = \left[\mathbf{x}_1^T, ..., \mathbf{x}_{n_T/2}^T \right]^T$ be the $n_T \times 1$ vector of transmitted signal. To simplify the representation, the time index is dropped. The channel model is then,

$$\mathbf{r} = \mathbf{Hx} + \mathbf{n},$$

where $\mathbf{r}$ is the $n_R \times 1$ vector of received signal; $\mathbf{H}$ is the $n_R \times n_T$ channel gain matrix; $\mathbf{n}$ is AWGN.

Before the OSIC algorithm is presented, several variables are defined. Let $\mathbf{H}[k]$ denote the channel gain matrix of the k-th layer, which is composed of the $2k$-th and the $(2k+1)$-th column of $\mathbf{H}$. Let $\mathbf{H}[m,n]$ denote the channel gain matrix pertaining to the layers from m to n. Also let $\mathbf{H}[m,n \mid i]$ denote the channel gain matrix pertaining to the layers from m to n, except layer i.

Without loss of generality, it is assumed that at the k-th stage of OSIC, layers $1, ..., k-1$ have been detected without error. Denote the detected and decoded symbols as $\widehat{\mathbf{c}}[1, k-1] = \left[\widehat{\mathbf{c}}_1^T, ..., \widehat{\mathbf{c}}_{k-1}^T \right]^T$ and the corresponding the signal after TVLT $\widehat{\mathbf{x}}[1, k-1] = [\widehat{\mathbf{x}}_1, ..., \widehat{\mathbf{x}}_{k-1}]^T$. Then the channel observations pertaining to layers k to $n_T/2$ are obtained by removing the contributions of layers 1 to $k-1$:

$$\begin{aligned}
\mathbf{r}[k, n_T/2] &= \mathbf{r} - \mathbf{H}[1, k-1]\,\widehat{\mathbf{x}}[1, k-1] \\
&= \mathbf{H}[k, n_T/2]\,\mathbf{x}[k, n_T/2] + \mathbf{n},
\end{aligned}$$

where $\mathbf{x}[k, n_T/2]$ is the signal transmitted from the layers k to $n_T/2$.

To detect the next layer, the signal for the other undetected layers should be nulled. Assume the i-th layer, $k \leq i \leq n_T/2$ is going to be detected. After nulling the signals from other layers, the signals of the i-th layer is

$$\begin{aligned}
\mathbf{y}[i] &= \mathbf{\Phi}[i]^\dagger \mathbf{r}_k \\
&= \mathbf{\Phi}[i]^\dagger \mathbf{H}[k, n_T/2]\,\mathbf{x}[k, n_T/2] + \mathbf{\Phi}_i^\dagger \mathbf{n} \\
&= \mathbf{\Phi}[i]^\dagger \mathbf{H}[i]\,\mathbf{x}[i] + \mathbf{\Phi}_i^\dagger \mathbf{n} \\
&\triangleq \overline{\mathbf{H}}[i]\,\mathbf{x}[i] + \mathbf{z}
\end{aligned}$$

where $\mathbf{\Phi}[i]$ is the projection to the null space of $\mathbf{H}[k, n_T/2 \mid i]$ whose columns are normalized; $\overline{\mathbf{H}}[i] \triangleq \mathbf{\Phi}_i^\dagger \mathbf{H}[i]$ is the post projection channel gain matrix for the i-th layer; $\mathbf{z} \triangleq \mathbf{\Phi}[i]^\dagger \mathbf{n}$ is the transformed noise term. Since the columns

of $\Phi[i]$ is normalized, the variance of the noise is not changed after the projection. The matrix $\Phi[i]$ is obtained by first computing

$$\Psi[i] = I - H[k, n_T/2 \mid i] \left(H[k, n_T/2 \mid i]^\dagger H[k, n_T/2 \mid i]\right)^{-1} H[k, n_T/2 \mid i]^\dagger,$$

and then normalize its columns.

To minimize the error rate, the detection order should be determined. That is, the layer with the least error probability should be detected first. For conventional layered space-time codes [5], ordering is not applicable since it is difficult to predict which layer, with the post projection channel $\overline{H}[i]$, $i = k, ..., n_T/2$, will have the least probability of error.

For turbo STC with TVLT, whether or not the decoder for a specific layer will converge to the correct decision, can be predicted with high accuracy by checking whether the eigenvalues $(\lambda_1[i], \lambda_2[i])$ of $\frac{E_s}{n_T}\overline{H}[i]^\dagger \overline{H}[i]$ fall in the region of convergence, as shown in Figure 3.6. Then the layer that is predicted to converge should be detected first. If for multiple layers the eigenvalues $(\lambda_1[i], \lambda_2[i])$ fall in the convergence region, the layer that should be detected first is determined as follows. Given an arbitrary $\lambda_1[i]$, let $\lambda_{2,\min}(\lambda_1[i])$ be the minimum required λ_2 for the i-th decoder to converge. Then the k-th layer with

$$k = \arg \max_i \left(\lambda_2[i] - \lambda_{2,\min}(\lambda_1[i])\right).$$

should be detected first. That is, the layer whose eigenvalues are the farthest away from the border between the region of convergence and region of non-convergence should be detected first.

5.2.3   Numerical Results

In this section the simulation results for the proposed H-LTST scheme are presented. In H-LTST, TVLT is employed at the transmitter which in turn enables the OSIC. For comparison, the performances of two other systems are also shown. One system does not employ TVLT and consequently can only perform SIC without ordering. This system has a similar structure with the conventional LSTC [5]. Another system employs TVLT but still performs SIC without ordering although ordering is available. By comparing the performance of H-LTST with those of the two other systems, the effects of TVLT and OSIC will be clearly shown.

83

The turbo-STC encoder used in all systems are Code 1 from Table 3.1 with interleaver length 1024. This is a rate 3/6 encoder with 8-PSK modulation. Simulations results will be shown for four transmit antenna four receive antenna (4×4) and eight transmit antenna eight receive antenna (8×8) configurations. The data rates of these two configurations are 6 b/s/Hz and 12 b/s/Hz, respectively.

The FER performances of the 4×4 systems are shown in Figure 5.6. It is observed that H-LTST achieves more diversity than the two other systems. At FER=0.01, H-LTST outperforms the systems with no TVLT and no ordering by 2.5 dB, and outperforms the system with TVLT but no ordering by 2.0 dB. This comparison shows the importance of ordering in SIC detection, and demonstrates the advantage of H-LTST over conventional LSTC [5] which employs SIC detection but ordering is not available. It can also be observed that the system with TVLT but no ordering achieves more diversity than the system with neither TVLT nor ordering, but the FER performance improvement caused by the diversity improvement is limited. The reason is that although TVLT can guarantee full transmit diversity of each layer, with four receive antennas in the systems which already leads to a high order receive diversity, whether or not full transmit diversity is achieved will not cause significant performance difference.

The FER performance of the 8×8 systems are shown in Figure 5.7. In this case, H-LTST still achieves more diversity than the other systems. At FER=0.01, it outperforms the system with no TVLT and no ordering by 4 dB, and outperforms the systems with TVLT but no ordering by 3 dB. The more performance improvement in 8×8 case than in 4×4 case shows that as the number of transmit antenna ,or layers, increases, ordering in SIC plays a more important role. It can be also observed that only applying TVLT to each layer without using OSIC will lead only limited performance improvement.

5.3 Chapter Summary

In this chapter, two types of layered turbo space-time coding schemes, V-LTST and H-LTST are proposed for MIMO systems with large number of transmit antennas. The performance of the proposed schemes have been compared to existing layered MIMO schemes.

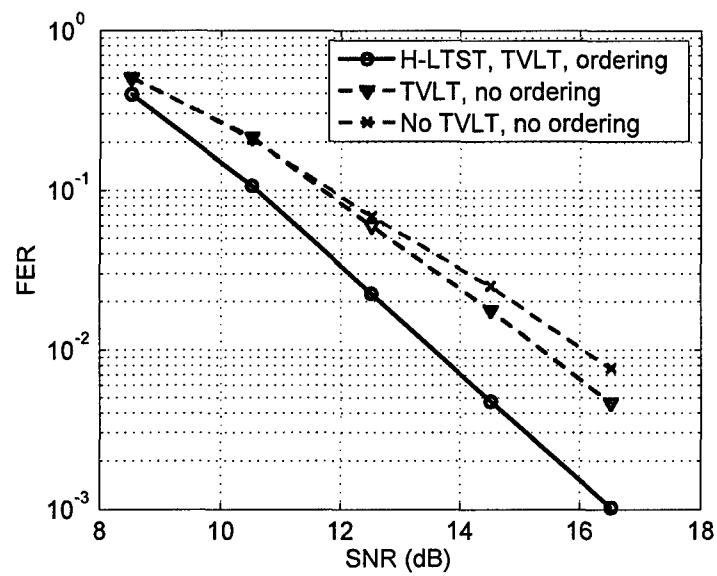V-LTST is proposed for systems with low order modulation and low data

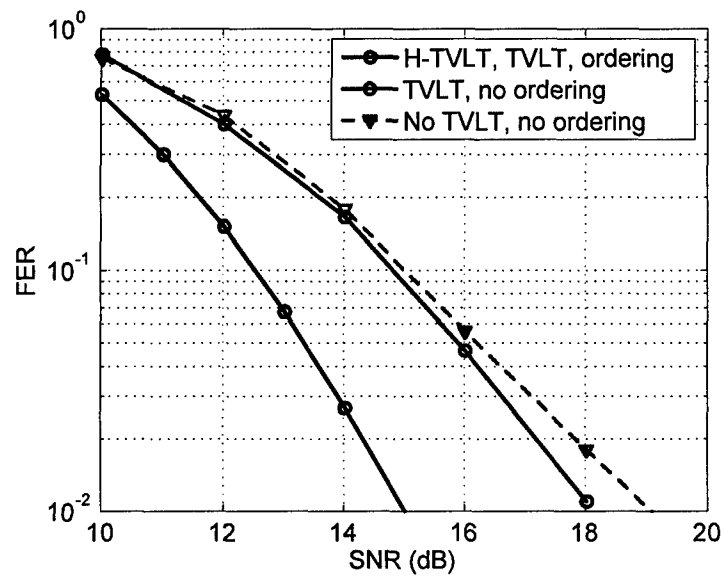Figure 5.6: Performance of H-LTST, 4 × 4, 6 b/s/Hz, with comparison to other schemes.

Figure 5.7: Performance of H-LTST, 8×8, 12 b/s/Hz, with comparison to other schemes.

rate per layer. With two antennas per layer structure, the number of interferers for each layer is reduced compared to the BLAST systems. Space interleaving is applied to further reduce the interference between layers. To maximize the coding gain, multidimensional set partition is applied to the encoder design. With these design techniques, the resultant V-LTST scheme avoids high complexity signal separation algorithms such as MMSE and ML, by performing only low complexity PIC in conjunction with turbo coding. It is shown that V-LTST achieves performance within 2 dB of outage capacity, but with significantly less complexity than other MIMO schemes with similar performances.

H-LTST is proposed for systems with high order modulation and high data rate per layer. At the transmitter, TVLT is applied at each layer with turbo-STC. Because of the TVLT used at each layer, whether or not the decoder of each layer will converge can be predicted based on the eigenvalues of the channel gain matrix of each layer. Hence the detection/decoding order can be determined. Simulation results show that H-LTST achieves significant performance improvement upon layered space-time coding without ordered detection/decoding.

Performance improvements by the proposed schemes have been demonstrated by comparing them to other existing schemes. It is also worth comparing V-LTST with H-LTST. The major advantage of V-LTST is that it is more suitable for communication systems with short delays. It is known that turbo-STC works well only when the codeword/interleaver is long enough. For a system with K channel use per frame, the length of the codeword transmitted using V-LTST is $Kn_T/2$ since signals transmitted from all layers belong to a single turbo-STC encoder. With H-LTST, each layer uses an independent encoder, the length of the codeword transmitted in each frame equal to K. The advantage of H-LTST is that it can be applied to systems with high order modulation while V-LTST is only suitable for low order modulation systems.

Chapter 6

Summary and Future Work

In wireless communications, space is said to be the final frontier. It has been shown that MIMO systems and techniques can lead to a big increase in system performance in terms of capacity, coverage and signal quality, all of which ultimately lead to increased spectrum efficiency. While the future is promising, there are still problems that need to be solved. The goal of this report is to propose a new class of turbo space-time codes with the application of TVLT. Compared to the existing space-time codes, the new codes proposed in this report can be designed with a significantly lower complexity procedure, while achieving a higher data rate and better performance. The new codes can also be extended and applied to systems with a very high data rate and a large number of transmit antennas.

The major contributions of this report include the following.

- The effects of the TVLT technique on the diversity gain and coding gain of turbo space-time codes are studied. It has been shown that with TVLT full diversity and good coding gain is achieved with high probability. The probability that these design goals are not met decreases exponentially with the minimum Hamming distance between the codewords. Hence, the need to test every pair of codewords for the rank criterion and coding gain criterion [1] is eliminated. The design criterion for turbo-STC with TVLT is to maximize the Hamming distance. Turbo-STCs are thus good candidates to be used with TVLT to achieve good coding gain, since they usually have large minimum Hamming distance following the existing design guidelines. Hence, the design of full diversity, good coding gain turbo-STCs is significantly

simplified.

- The effect of TVLT on the achievable rate of turbo-STC is studied. It is shown that while achieving full diversity, turbo-STC can achieve much higher data rate than what can be achieved by any full diversity space-time codes with constant modulation [1]. A new rate limit for turbo-STC with TVLT is proposed.

- The convenient and powerful EXIT chart method [13] is extended to analyze and predict the performance of turbo-STC with TVLT. It is shown that with TVLT the performance of turbo-STC is only determined by the singular values of the channel gain matrix. This reduction in effective channel parameters enables a low dimension description of the MIMO channel conditions, which further enables a low complexity search, with the EXIT chart method, for the channel conditions over which the turbo-STC decoder will converge. The FER performance of turbo-STC, can then be predicted with significantly lower complexity than which is needed for a full simulation. The low complexity performance analysis and prediction can significantly expedite the code comparison and selection in turbo-STC design.

- Multilevel turbo-STC with TVLT is proposed to increase the data rate without exponentially increasing the decoding complexity. Multidimensional set partition is applied which enables higher level codes to have higher data rate and/or lower trellis complexity. An iterative multi-stage decoder is proposed and reduced complexity decoder with a list sphere decoder is also proposed as an alternative.

- Layered turbo space-time (LTST) coding is proposed for MIMO systems with large number of transmit antennas, to avoid exponentially increasing decoding complexity with the number of transmit antennas. Two different structures, V-LTST and H-LTST, are proposed for systems with low and high order modulation, respectively. In V-LTST a very low complexity interference cancellation technique is used while superior performance is achieved. In H-LTST, ordered SIC is implemented, enabled by the TVLT application to each layer. Significant performance improvement is demonstrated compared to the conventional layered space-time coding structure where ordering is not available in the SIC detection.

89

- A group of new codes is constructed based on the design techniques proposed in this report. Their simulation results are reported.

Although much study has been done in this report on turbo-STC with TVLT scheme, the potential of this scheme are far from being fully explored. Anticipated future work may contain the following.

- Use turbo-STC with TVLT scheme to construct adaptive modulation and coding (AMC) MIMO systems. With TVLT, whether the turbo-STC decoder will converge or not can be accurately predicted based on the channel state information. The receiver can inform the transmitter to select a code with the maximum rate that guarantees the convergence of the decoder.

- Evaluate the possibility of applying turbo-STC with TVLT as a multiple access method for multi-user, MIMO systems. The sequence of pseudo-random unitary matrices used in TVLT can be regarded as the random codes for different users in CDMA systems.

- Study the applications of turbo-STC with TVLT to construct secured MIMO wireless systems. With the TVLT, the transmitted signals are multiplied by time varying pseudo-random unitary matrices and they appear random. The signals will be difficult to decode unless the random matrices are known.

- Evaluate the performance of turbo-STC with TVLT in multiple input multiple output orthogonal frequency division multiplexing (MIMO-OFDM) systems. OFDM technology is playing a more and more important role in broadband wireless communications. It has been applied to standards IEEE 802.11a/g/n and DVB-H, and will be used in other standards such as IEEE 802.16 and 802.20. Over the frequency selective channel, the minimum Hamming distance requirement of the code used with TVLT may be lowered. If this is true, the application of TVLT can be extended to conventional STC coded MIMO-OFDM systems.

Bibliography

[1] V. Tarokh and A. Seshadri, "Space-time codes for high data rate wireless communication: Performance criterion and code construction," *IEEE Trans. on Info. Theory*, vol. 44, pp. 744–765, March 1998.

[2] G. J. Foschini and M. J. Gans, "On limits of wireless communications in a fading environment when using multiple antennas," *Wireless Personal Communications, Kluwer Academic Publishers*, vol. 6, pp. 311–335, March 1998.

[3] E. Telatar, "Capacity of multi-antenna gaussian channels," *Eur. Trans. Telecomm. ETT*, vol. 10, pp. 585–596, Nov. 1999.

[4] V. Tarokh and H. Jafarkhani, "Space-time block coding for wireless communications: Performance results," *IEEE J. on Select. Areas Commun.*, vol. 17, pp. 451–460, March 1999.

[5] V. Tarokh and A. Naguib, "Combined array processing and space-time coding," *IEEE Trans. on Info. Theory*, vol. 45, pp. 1121–1128, May 1999.

[6] C. Berrou, A. Glavieux, and P. Thitimajshima, "Near shannon limit error-correcting coding and decoding: Turbo-codes," *in Proc. IEEE ICC '93*, vol. 2, pp. 1064–1070, 1993.

[7] D. Cui and A. Haimovich, "Performance of parallel concatenated space-time codes," *IEEE Commun. Lett.*, vol. 5, pp. 236–238, June 2001.

[8] Y. Liu, P. Fitz, and O. Y. Takeshita, "Full rate space-time turbo codes," *IEEE J. on Select. Areas Commun.*, vol. 19, pp. 969–980, May 2001.

[9] A. Stefanov and T. M. Duman, "Turbo-coded modulation for systems with transmit and receive antenna diversity over block fading channels: system model, decoding approaches, and practical considerations," *IEEE J. on Select. Areas Commun.*, vol. 19, pp. 958–968, May 2001.

[10] S. Baro and G. Bauch, "Improved codes for space-time trellis-coded modulation," *IEEE Commun. Lett.*, vol. 4, pp. 20–22, Jan. 2000.

[11] P. Robertson and T. Worz, "Bandwidth-efficient turbo trellis-coded modulation using punctured component codes," *IEEE J. on Select. Areas Commun.*, vol. 16, pp. 206–218, Feb 1998.

[12] C. Fragouli and R. Wesel, "Turbo-encoder design for symbol-interleaved parallel concatenated trellis-coded modulation," *IEEE Trans. on Commun.*, vol. 49, pp. 425–435, March 2001.

[13] S. T. Brink, "Convergence behavior of iterative decoded parallel concatenated codes," *IEEE Trans. on Commun.*, vol. 49, pp. 1727–1737, Oct. 2001.

[14] H. E. Gamal and A. R. Hammons, "Analyzing the turbo decoder using Gaussian approximation," *IEEE Trans. on Info. Theory*, vol. 47, pp. 671–686, Feb. 2001.

[15] D. Divsalar, S. Donlinar, and F. Pollara, "Iterative turbo deocder analysis based on density evolution," *IEEE J. on Select. Areas Commun.*, vol. 19, pp. 891–907, May 2001.

[16] A. Grant, "Convergence of non-binary iterative decoding," *in Proc. IEEE GLOBECOM '01*, vol. 2, pp. 1058–1062, Nov 2001.

[17] G. Ungerboeck, "Channel coding with multilevel/phase signals," *IEEE Trans. on Info. Theory*, vol. 28, pp. 55–67, Jan. 1982.

[18] A. Wittneben, "A new bandwidth efficient transmit antenna modulation diversity scheme for linear digital modulation," *in Proc. IEEE ICC' 93*, vol. 3, pp. 1630–1634, May 1993.

[19] A. Hiroike, F. Adachi, and N. Nakajima, "Combined effects of phase sweeping transmitter diversity and channel coding," *IEEE Trans. on Veh. Technol.*, vol. 41, pp. 170–176, May 1992.

[20] B. Su and S. Wilson, "Phase sweeping transmitter diversity in mobile communications," *in Proc. IEEE VTC '96*, vol. 1, pp. 131–135, April 1996.

[21] X. Ma and G. B. Giannakis, "Space-time-multipath coding using digital phase sweeping," *in Proc. IEEE GLOBECOM '02*, vol. 1, pp. 384–388, Nov 2002.

[22] A. Gutierrez, J. Li, S. Baines, and D. Bevan, "An introduction to PSTD for is-95 and cdma2000," *IEEE Wireless Communications and Networking Conference, WCNC'99*, vol. 3, pp. 1358–1362, Sept. 1999.

[23] W. Shi, C. Komninakis, R. Wesel, and B. Daneshrad, "Robustness of space-time turbo codes," *in Proc. IEEE ICC '01*, vol. 6, pp. 11–14, June 2001.

[24] H. Chen and A. Haimovich, "Exit charts for turbo trellis coded modulation," *IEEE Commun. Lett.*, vol. 8, pp. 668–670, Nov. 2004.

[25] C. D. Meyer and C. Meyer, "Matrix analysis and applied linear algebra," *Society for Industrial and Applied Math*, p. 457, February 2001.

[26] L. C. Perez, J. Seghers, and D. J. Costello Jr., "A distance spectrum interpretation of turbo codes," *IEEE Trans. on Info. Theory*, vol. 42, pp. 1698–1709, Nov. 1996.

[27] A. Perotti and S. Benedetto, "A new upper bound on the minimum distance of turbo codes," *to appear in IEEE Trans. on Info. Theory*. available at http://commgroup.polito.it/personal/perotti/pubs/dmin-ub.pdf.

[28] S. G. Wilson, "Digital modulation and coding," *Prentice-Hall, Inc.*, pp. 432–434, 1996.

[29] S. S. Pietrobon, R. H. Deng, A. Lafanechere, G. Ungerboeck, and D. J. Costello Jr., "Trellis-coded multidimensional phase modulation," *IEEE Trans. on Info. Theory*, vol. 36, pp. 63–89, Jan 1990.

[30] M. Chiani, M. Z. Win, A. Zanella, and J. H. Winters, "Exact symbol error probability for optimum combining in the presence of multiple cochannel interferers and thermal noise," *in Proc. IEEE GLOBECOM '01*, vol. 2, pp. 1182–1186, 2001.

[31] H. Imai and S. Hirakawa, "A new multilevel coding method using error-correcting codes," *IEEE Trans. on Info. Theory*, vol. IT-23, pp. 371–377, May 1977.

[32] L.-J. Lampe, R. Schober, and R. Fischer, "Multilevel coding for multiple-antenna transmission," *IEEE Trans. on Wireless Commun.*, vol. 3, pp. 203–208, Jan. 2004.

[33] U. Wachsmann, R. Fischer, and J. Huber, "Multilevel codes: theoretical concepts and practical design rules," *IEEE Trans. on Info. Theory*, vol. 45, pp. 1361–1391, July 1999.

[34] D. Cui and A. Haimovich, "Design and performance of turbo space-time coded modulation," *IEEE GLOBECOM 2000*, vol. 3, pp. 1627–1631, 2000.

[35] L. Bahl, J. Cocke, F. Jelinek, and J. Raviv, "Optimal decoding of linear codes for minimizing symbol error rate," *IEEE Trans. on Info. Theory*, vol. 20, pp. 284–287, Mar 1974.

[36] B. M. Hochwald and S. ten Brink, "Achieving near-capacity on a multiple-antenna channel," *IEEE Trans. on Commun.*, vol. 51, pp. 389–399, March 2003.

[37] G. J. Foschini, "Layered space-time architecture for wireless communication in fading environments when using multiple antennas," *Bell Labs Tech Journal*, pp. 41–59, Autumn 1996.

[38] P. W. Wolniansky, G. J. Foschini, G. D. Golden, and R. A. Valenzuela, "V-BLAST: An architecture for realizing very high data rates over rich-scattering wireless channel," *in Proc. IEEE ISSSE*, 1998.

[39] M. Sellathurai and S. Haykin, "A simplified diagonal BLAST architecture with iterative parallel-interference cancelation receivers," *in Proc. IEEE ICC 2001*, vol. 10, pp. 3067–3071, June 2001.

[40] H. E. Gamal and A. R. Hammons Jr., "A new approach to layered space-time coding and signal processing," *IEEE Trans. on Info. Theory*, vol. 47, pp. 2321–2334, Sept. 2001.

[41] A. A. AlRustamani, A. Stefanov, and B. R. Vojcic, "Turbo-greedy coding for multiple antenna systems," *in Proc. IEEE ICC '01*, vol. 6, pp. 1684–1689, 2001.

[42] X. Li, H. Huang, G. J. Foschini, and R. A. Valenzuela, "Effects of iterative detection and decoding on the performance of BLAST," *in Proc. IEEE GLOBECOM '00*, vol. 2, pp. 1061–1066, Nov. 2000.

[43] M. Tao and R. Cheng, "Improved design criteria and new trellis codes for space-time coded modulation in slow flat fading channels," *IEEE Commun. Lett.*, vol. 5, pp. 313–315, July 2001.